Defining Specificity Determinants of cGMP Mediated Gustatory Sensory Transduction in *Caenorhabditis elegans*

Heidi K. Smith,* Linjiao Luo,† Damien O'Halloran,‡ Dagang Guo,§ Xin-Yun Huang,§ Aravinthan D. T. Samuel,† and Oliver Hobert*,†,1

*Department of Biochemistry and Molecular Biophysics, Howard Hughes Medical Institute, Columbia University Medical Center, New York, New York 10032, †Department of Physics and Center for Brain Science, Harvard University, Cambridge, Massachusetts 02138, ‡Department of Biological Sciences and Institute for Neuroscience, George Washington University, Washington DC, 20037, and §Department of Physiology, Cornell University Weill Medical College, New York, New York 10065

ABSTRACT Cyclic guanosine monophosphate (cGMP) is a key secondary messenger used in signal transduction in various types of sensory neurons. The importance of cGMP in the ASE gustatory receptor neurons of the nematode *Caenorhabditis elegans* was deduced by the observation that multiple receptor-type guanylyl cyclases (rGCs), encoded by the *gcy* genes, and two presently known cyclic nucleotide-gated ion channel subunits, encoded by the *tax-2* and *tax-4* genes, are essential for ASE-mediated gustatory behavior. We describe here specific mechanistic features of cGMP-mediated signal transduction in the ASE neurons. First, we assess the specificity of the sensory functions of individual rGC proteins. We have previously shown that multiple rGC proteins are expressed in a left/right asymmetric manner in the functionally lateralized ASE neurons and are required to sense distinct salt cues. Through domain swap experiments among three different rGC proteins, we show here that the specificity of individual rGC proteins lies in their extracellular domains and not in their intracellular, signal-transducing domains. Furthermore, we find that rGC proteins are also sufficient to confer salt sensory responses to other neurons. Both findings support the hypothesis that rGC proteins are salt receptor proteins. Second, we identify a novel, likely downstream effector of the rGC proteins in gustatory signal transduction, a previously uncharacterized cyclic nucleotide-gated (CNG) ion channel, encoded by the *che-6* locus. *che-6* mutants show defects in gustatory sensory transduction that are similar to defects observed in animals lacking the *tax-2* and *tax-4* CNG channels. In contrast, thermosensory signal transduction, which also requires *tax-2* and *tax-4*, does not require *che-6*, but requires another CNG, *cng-3*. We propose that CHE-6 may form together with two other CNG subunits, TAX-2 and TAX-4, a gustatory neuron-specific heteromeric CNG channel complex.

THE identification and subsequent molecular characterization of mutant *Caenorhabditis elegans* strains defective in sensing specific environmental parameters has revealed many components of signal transduction pathways in sensory neurons (Bargmann 2006; Sengupta 2007). Among the genes identified by mutant analysis are those coding for several distinct cyclic guanosine monophosphate (cGMP)-generating guanylyl cyclases (GCs), cGMP-dependent protein kinase, as well as cyclic nucleotide-gated (CNG) channels (Coburn and Bargmann 1996; Komatsu *et al.* 1996; Birnby *et al.* 2000; Daniels *et al.* 2000; L'Etoile and Bargmann 2000; Cheung *et al.* 2004; Gray *et al.* 2004; Inada *et al.* 2006; Pradel *et al.* 2007; Ortiz *et al.* 2009). These genes are expressed in different types of sensory neurons and are required for sensation of odorants, gustatory cues, temperature, bacterial pathogens, and ambient oxygen levels. cGMP has therefore emerged as a key signal transducer for various sensory modalities.

While the cGMP dependence of many sensory systems is now well established, sensory receptors that trigger the cGMP-dependent signaling cascades are only characterized only for some, but not all sensory modalities. In *C. elegans*, seven transmembrane olfactory receptors as well as photoreceptors couple to GCs and CNGs via heterotrimeric G proteins (Bargmann

doi: 10.1534/genetics.113.152660
Manuscript received April 27, 2013; accepted for publication May 18, 2013
Supporting information is available online at http://www.genetics.org/lookup/suppl/doi:10.1534/genetics.113.152660/-/DC1.
OH dedicates this paper to the memory of the late Professor Alberto Mancinelli.
[1]Corresponding author: Columbia University Medical Center, 701 W. 168 th St., HHSC 724, New York, NY 10032. E-mail: or38@columbia.edu

2006; Liu *et al.* 2010). How other cGMP-dependent sensory modalities, such as taste or temperature, are coupled to GCs and CNGs is not understood simply because the respective receptor systems have not been well defined.

Taste is often categorized into five modalities: sweet, bitter, salty, sour, and umami (the taste of glutamate or amino acids). In vertebrates and invertebrates, sweet, bitter, and umami tastes are thought to be sensed by specific types of G-protein-coupled receptors (GPCRs) (Scott 2005). Attractive responses to low salt concentrations are mediated by ion channels of the epithelial sodium channel (EnaC) type (Chandrashekar *et al.*, 2010). However, vertebrate ENaC channels are sodium selective, yet worms sense distinct types of salt cations and anions (Ward 1973; Ortiz *et al.* 2009); moreover, amiloride does not block the behavioral response of *C. elegans* to NaCl (Hukema 2006). Therefore, salt receptor molecules remain to be identified in *C. elegans*.

The ASE neurons, consisting of a pair of morphologically symmetric cells (ASEL and ASER) are the main taste receptor neurons in *C. elegans*. Laser ablation analysis demonstated that they are required to process a variety of distinct taste cues, including amino acids, salts, and other small molecules (Bargmann and Horvitz 1991). Many and perhaps all of the cues that are processed by the ASE neurons are sensed in a left/right asymmetric manner and also trigger distinct outputs (Pierce-Shimomura *et al.* 2001; Suzuki *et al.* 2008; Ortiz *et al.* 2009). For example, sodium ions are sensed by the ASEL neuron and trigger run behavior upon increases in sodium concentration, while chloride ions are sensed by the ASER neuron and trigger turning behavior upon decreases in chloride concentration (Suzuki *et al.* 2008). Previous genetic analyses have identified two CNG channel subunits, encoded by the ASEL/R-expressed *tax-2* and *tax-4* genes, as being required for all ASE-mediated sensory processes (Coburn and Bargmann 1996; Komatsu *et al.* 1996). Moreover, we have previously shown that cGMP-generating, receptor-type guanylyl cyclase (rGC) proteins, encoded by the *gcy* genes, are required for sensing a number of distinct salt ions (Ortiz *et al.* 2009). Curiously, with almost 30 representatives, rGC-encoding *gcy* genes have significantly expanded in *Caenorhabditis* genomes and almost one-third of them are expressed in a left/right asymmetric manner in the ASEL and ASER neurons (Ortiz *et al.* 2006).

Genetic loss-of-function analysis has shown that specific *gcy* genes endow ASEL and ASER with the ability to sense specific distinct salt ions (Figure 1A) (Ortiz *et al.* 2009). For example, ASER-expressed *gcy-1* is required to efficiently respond to potassium, but not other salt ions, while *gcy-4* is required for animals to respond efficiently to bromide and iodide ions (Ortiz *et al.* 2009). The sensory modality-specific function of *gcy* genes was unanticipated since work in other systems (*e.g.*, the vertebrate retina; Koch *et al.* 2002) or worm olfactory and photosensory neurons (Bargmann 2006; Liu *et al.* 2010) suggests that rGC proteins may only serve as intermediary signal transducers that are activated by sensory modality-specific GPCRs through G proteins. The

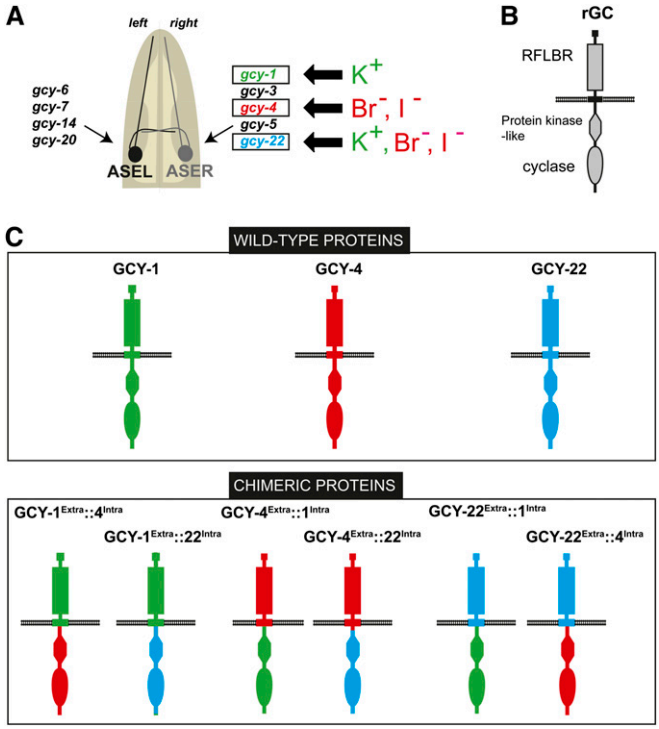

Figure 1 GCY protein function. (A) Expression and function of *gcy* genes in the ASE gustatory neurons, as previously reported (Ortiz *et al.* 2006, 2009). (B) Schematic depiction of rGC domains. (C) Schematic of rGC chimeras generated and tested in this study.

observation that individual *C. elegans* rGC proteins act to transduce specific salt sensory information within the ASE neurons suggests the intriguing possibility that transmembrane rGC proteins themselves may serve as salt receptor proteins. Receptor functions for rGC proteins are indeed well characterized in the vertebrate system, though not in sensory function. Rather, vertebrate rGC proteins act as receptors for small peptides in several distinct tissue types; these peptides stimulate the intracellular rGC activity of the receptor protein (Wedel and Garbers 2001; Potter 2011).

In this article, we further investigate the hypothesis that *C. elegans* rGC proteins may themselves be salt receptors. To address this hypothesis, we asked whether the specificity in rGC function lies in their extracellular domain, as one would expect if they were receptor proteins, or whether specificity lies in their intracellular domain. The latter would be consistent with a possibility in which different rGC proteins couple to distinct upstream signaling inputs. We also test whether their ectopic expression in other sensory neurons endows these neurons with the capacity to respond to specific salt ions.

In an attempt to shed more light on rGC-mediated signal transduction in the ASE neurons, we also determined the molecular identity of a novel regulator of gustatory signal transduction, encoded by the *che-6* gene. *che-6* was identified as a chemotaxis mutant >30 years ago (Lewis and Hodgkin 1977). We find that *che-6* encodes a CNG channel that likely acts directly downstream of rGC proteins. While

this CNG is required for ASE salt transduction, it is not required for the transduction of several other sensory cues in other sensory neurons, in which we implicate instead a previously uncharacterized *cng* gene, *cng-3*.

Materials and Methods

Mutant alleles

che-5(e1073)IV, *che-6(e1126)IV*, *che-7(e1128)V* (Lewis and Hodgkin 1977), *gcy-22(tm2364)V*, *gcy-4(tm1653)II*, *gcy-1 (tm2669)II* (Ortiz *et al.* 2009), *che-1(ot66)I*, *cng-3(jh113) IV* (Cho *et al.* 2004), *tax-2(ot25)I* (Sarin *et al.* 2007), *tax-4 (p678)III* (Dusenbery *et al.* 1975), and *che-6(tm5036)IV* were kindly provided by Shohei Mitani, National Bioresource Project, Japan, and *che-7(ok2373)V* was kindly provided by the Oklahoma and Vancouver *C. elegans* knock out consortium.

DNA constructs for transgenic line construction

A list of transgenic lines can be found in Supporting Information, File S1.

Expression wild-type and chimeric GCY receptors: The full-length rescue constructs carried by strains (*gcy-1(tm2669)II*; *otEx5076*, *gcy-4(tm1653)II*; *otEx5101*, *gcy-22(tm2364)V*; *otEx5120)* for *gcy-1*, *gcy-4*, and *gcy-22*, respectively, were made by using a PCR fragment covering the entire gene locus and injected into the *gcy-1*, *gcy-4*, and *gcy-22*, mutant background, respectively, as a simple array at 15 ng/μl with 5 ng/μl *elt-2*::*gfp* as a co-injection marker.

Chimera constructs were made by fusing PCR fragments from N2 genomic DNA that encode the extracellular domain and transmembrane domain of one GCY to the intracellular domain of another. Domains were predicted with the SMART server (Letunic *et al.* 2012). The junction sites for the individual GCY proteins are:

GCY-1: .....[.... LIMIIGCLCVI]$_{trans}$[GKRAERARI.....]$_{intra}$
GCY-4: .....[....AIAVTILILLAIII]$_{trans}$ [CMSSKIRNRR...]$_{intra}$
GCY-22: .....[....AAALVLIIAVISTI]$_{trans}$ [VFLVRSKRQE...]$_{intra}$.

The resulting chimeric PCR products was then subcloned into pPD95.75 with the ASER-specific *gcy-5* promoter (containing the sequence 305 bp upstream of the *gcy-5* translational start site) using the restriction sites, added onto the PCR primers (noted below). The sites were designed to allow removal of GFP from the vector. Chimeras containing the extracellular domain of a specific GCY protein were injected into animals mutant for the respective *gcy* gene (at 25 ng/μl of DNA as a simple array together with 50 ng/μl of the *elt-2*::*gfp* marker). Three lines were scored for chemotaxis behavioral rescue and subsequently crossed into the *gcy* mutant background that matches the intracellular domain of the respective chimera and then tested for rescue of behavioral phenotypes. The *gcy* mutant genotypes were followed by PCR. Plasmids are as follows:

pHKS015: *gcy-5*^{prom}::*gcy-4*$^{Extra(aa1\text{-}aa518)}$::*gcy-22*$^{Intra(aa462\text{-}aa1012)}$], cloned into pPD95.75, using *Kpn*I/*Eco*RI, injected into *gcy-4(tm1653)* and crossed into *gcy-22 (tm2364)*. Array names: *otEx5102-otEx5104*.

pHKS016: [*gcy-5*^{prom}::*gcy-22*$^{Extra(aa1\text{-}aa461)}$::*gcy-4*$^{Intra(aa519\text{-}aa1143)}$], cloned into pPD95.75, using AgeI/*Eco*RI, injected into *gcy-22(tm2364)* and crossed into *gcy-4 (tm1653)*. Array names: *otEx5105-otEx5107*.

pHKS017: [*gcy-5*^{prom}::*gcy-4*$^{Extra(aa1\text{-}aa518)}$::*gcy-1*$^{Intra(aa520\text{-}aa1137)}$], cloned into pPD95.75, using *Kpn*I/*Eco*RI, injected into *gcy-4(tm1653)* and crossed into *gcy-1 (tm2669)*. Array names: *otEx5086-otEx5088*.

pHKS018: [*gcy-5*^{prom}::*gcy-1*$^{Extra(aa1\text{-}aa519)}$::*gcy-4*$^{Intra(aa519\text{-}aa1143)}$], cloned into pPD95.75, using AgeI/*Eco*RI, injected into *gcy-1(tm2669)* and crossed into *gcy-4 (tm1653)*. Array names: *otEx5083-otEx5085*.

pHKS019: [*gcy-5*^{prom}::*gcy-1*$^{Extra(aa1\text{-}aa519)}$::*gcy-22*$^{Intra(aa462\text{-}aa1012)}$], cloned into pPD95.75, using AgeI/*Eco*RI, injected into *gcy-1(tm2669)* and crossed into *gcy-22 (tm2364)*. Array names: *otEx5077-otEx5079*.

pHKS020: [*gcy-5*^{prom}::*gcy-22*$^{Extra(aa1\text{-}aa461)}$::*gcy-1*$^{Intra(aa520\text{-}aa1137)}$], cloned into pPD95.75, using AgeI/*Eco*RI, injected into *gcy-22(tm2364)* and crossed into *gcy-1 (tm2669)*. Array names: *otEx5080-otEx5082*.

Pansensory heterologous expression: The *gcy-4* and *gcy-22* genomic loci (from start to stop codon) were PCR amplified from genomic DNA and subsequently subcloned into pPD95.75 containing the *osm-6* promoter (containing sequences 2083 bp upstream of the *osm-6* locus, relative to its translational start site) using the specific insertion sites noted below that removed the GFP from the vector. In both cases the DNA was injected at 25 ng/μl as a simple array and either *elt-2*::*DsRed* or *elt-2*::*gfp* was used as a co-injection marker at 50 ng/μl.

pHKS013: *osm-6*^{prom}::*gcy-4*, cloned into pPD95.75 using *Kpn*I/*Eco*RI. Array names: *otEx5067-otEx5069*.

pHKS014: *osm-6*^{prom}::*gcy-22*, cloned into pPD95.75 using AgeI/*Eco*RI. Array names: *otEx5070-otEx5072*.

ASI-specific heterologous expression: The *gcy-4* and *gcy-22* genomic loci (from start to stop codon) were PCR-amplified from genomic DNA and subsequently subcloned into the pPD95.77 vector containing the *srg-47* promoter, kindly provided by Piali Sengupta. In the case of the *gcy-4* and *gcy-22* alone the DNA was injected at 25 ng/μL as a simple array and *myo-2*::*gfp* was used as a co-injection marker at 2 ng/μL. In the case of the double injection, the *gcy-4* and *gcy-22* were each injected as simple arrays at 2.5 ng/μL each with *myo-2*::*gfp* as a co-injection marker at 3 ng/μL.

pHKS031: *srg-47*^{prom}::*gcy-4*, cloned into pPD95.77 using *Eag*I/*Kpn*I. Array names: *otEx5349*, *otEx5351*, *otEx5352*.

pHKS032: *srg-47*^{prom}::*gcy-22*, cloned into pPD95.77 using *Eag*I/*Kpn*I. Array names: *otEx5353-otEx5355*.

Array names for simultaneous injection of pHKS031 and pHKS032 are *otEx5358-otEx5361*.

Transformation rescue of che mutants: For *che-7* rescue, fosmid WRM0620bH04 was injected into *che-7(e1128)* animals at 5 ng/μL, 3 ng/μL *elt-2*::*gfp* as a co-injection marker as well as 130 ng/μL genomic bacterial array (array name: *otEx5063)*. The *che-6* mutant phenotype was rescued with a genomic DNA clone and by expression with a cell-type specific promoter. For the genomic rescue, the *che-6* locus was amplified from coordinates 2103929-2111708 (103 bp before the start site to 127 bp after the end of the last exon) by PCR and the PCR product was injected at 15 ng/μL with 5 ng/μL *elt-2*::*gfp* as a co-injection marker. Array names: *otEx5064-otEx5066*

che-6 forward: GAAGCCAGCATTGTCCTGAATG
che-6 reverse: CACTCCTATTACAGTCTGGTG

pHKS021 (*ceh-36*^{prom}::*che-6*) was generated using the pPD95.75 vector containing sequences 1852 bp upstream of the *ceh-36* locus, relative to its translational start site. The full length *che-6* that was generated by PCR from genomic N2 DNA was inserted using the AgeI/*Xho*I cut sites and the DNA was injected at 25 ng/μL as a simple array and 50 ng/μL of the *elt-2*::*gfp* marker. Array names: *otEx5154-otEx5156*.

che-6 reporter gene: The *che-6*^{prom}::*gfp* transcriptional reporter was made by PCR fusion as described previously (Hobert 2002). 772 bp of sequences upstream of *che-6* were fused by PCR to a *gfp*::*unc-54*$^{3'UTR}$ fragment using the two primers "*che-6*^{prom}::*gfp* fusion forward" (GGGCAAATTCTGTGAACCATATTCCT) and "*che-6*^{prom}::*gfp* fusion reverse" (GGAAACAGTTATGTTTGGTATATTGGG). The *gfp*::*unc-54*$^{3'UTR}$ fragment was PCR amplified from the plasmid pPD95.75. The resulting PCR fusion was PCR purified and injected into wildtype (N2) animals at 80 ng/μl alongside the co-injection marker *elt-2*::*gfp* at 50 ng/μl. The resulting transgenic array name is *hanEx24*.

Chemotaxis assays

Two types of chemotaxis assays were used: radial gradient assays and population assays. A radial gradient assay was used if transgenic extrachromosomal DNA-containing animals were scored so that individual transgenic worms could be picked and assayed. In this assay, four animals were placed around the circumference of a salt gradient 1 cm away from the peak formed by application of 10 μl of 1M salt attractant spotted 14–16 hr before assay and a second 4-μl drop of 1 M salt attractant spotted 3–4 hr before assay. This assay is modified from previous single worm tracking assays (Pierce-Shimomura *et al.* 2001).The plates used in this assay were identical to those used in the population assays except for the concentration of the gradient. After the worms were placed on the plate around the circumference of the gradient the recording started within 1 min. Behavior was recorded continuously for 15 min using a USB microscope (GSI High-Definition Scientific Digital LED Microscope) over the plate while the cover of the Petri dish remained on to avoid drying. A circle of red LED lights around the plate illuminated the worms while the assays were carried out in the dark to increase the contrast for scoring. The videos were converted to Quicktime movies and subsequently scored for time spent within the peak of the gradient. In this case the chemotaxis index (CI) was calculated as gradient tracking assay CI = (time in seconds spent in the peak for 4 worms)/(total time). The total time was 3,600 sec to account for four worms multiplied by the length of the assay (900 s). For these assays *n* represented the average of two assays done in duplicate on the same day. Therefore $n = 1$ represents the average of two plates.

The population assay is based on a protocol described previously (Chang *et al.* 2004; Ortiz *et al.* 2009), with some minor modifications. Buffered agar (20 g/L agar, 1 mM $CaCl_2$, 1 mM $MgSO_4$, 5 mM KPO_4) similar to the plates worms are maintained on for routine usage were used as assay plates with the exception of a saturating concentration of 100mM NH_4Ac added to counteract the NH_4^+ and Ac^- responses of individual ions. 10-cm diameter Petri dishes were filled with 10 mL and allowed to cool for 1–3 hr. A salt gradient was established opposite a control gradient (water) by adding 10 μl of 2.5 M salt solutions (adjusted to pH = 6 with either NH_4OH or acetic acid) to the attractant spot, and 10 μl of ddH_2O to the control spot. After 12–16 hr an additional 4 μL of salt solution and ddH_2O was added. After 4 hr the assays were carried out by adding between 50–250 synchronized adult worms that had been washed 3 times with M9 buffer. Using a glass Pasteur pipette the worms were transferred to the center of the plate with minimal liquid. The remaining liquid was removed with a tissue so the worms were using normal taxis across the plate and not swimming motion in remaining liquid. Two to five minutes before the worms are placed on the plate, 2 μl of 1M sodium azide was added to the salt spot as well as the control spot. The worms naturally disperse from the center point and explore the plate. When wild-type worms encounter the salt gradient they move up the gradient and this anesthetizes the worms and locks them into their position. The worms that moved across the control spot by chance are accounted for in the equation for the chemotaxis index. The worms were left at between 20–23° for exactly 1 hr before being placed at 4° to be counted the next day. The chemotaxis index (CI) was calculated as population assay CI = (# worms in attractant − # worms in control)/(total # of worms). Worms that failed to move from the center spot were not counted in the assay. Each *n* represented the average of two assays done in duplicate on the same day. In this manner, a hypothetical $n = 1$ represents 100–500 worms.

For odortaxis assay, we also used a population assay, essentially as previously described (Colburn and Bargmann 1996). Specifically, we used buffered agar plates (20 g/L agar, 1 mM $CaCl_2$, 1 mM $MgSO_4$, 5 mM KPO_4) for the assays

and placed between 50-100 synchronized worms at the center point. This assay is quite similar to the radial gradient population assay in that the odortaxis test spot is placed diametrically opposite to the control spot. The sodium azide (2 μl of 1 M) was added at the control and odor points. The worms are then allowed to explore the plate for 1 hr at room temperature and the sodium azide acts to anesthetize the worms at each spot. Because the assays tests for odor the droplets were placed on the cover of the plate and once the worms were placed in the center the plate was intverted onto the cover. The benzaldehyde was diluted to 1:200 in ethanol. The control spot placed opposite is of the odorant in this case is ethanol alone. The odortaxis index is calculated in the same manner as the population assays for salt chemotaxis.

Statistical analyses

All statistical tests were completed GraphPad Prism 6. The data for all behavioral assays of chemotaxis indices were represented as the mean ± SEM. Comparisons were made using Student's two-tailed *t*-test assuming equal variance when comparing less than 5 groups. When more than 2 comparisons were made a correction factor was utilized in the Student's *t*-test to adjust the *P*-value for multiple comparisons. When testing more than 5 comparisons a one-way ANOVA was used comparing the mean of each group with the mutant mean and the Holm–Sidak correction was applied. The Holm–Sidak correction or Bonferroni adjustment for multiple comparisons was used based on the number of comparisons being made and the *n* value to minimize the elimination of false positive without creating false negatives in the process.

Thermotaxis

Our linear thermal gradients apparatus is a larger and improved version of the one we previously designed (Ryu and Samuel 2002). Each end of an anodized aluminum slab (24 inches × 12 inches × ¼ inch) was fixed at a specific temperature under thermal electric control (Oven Industries). A 22 cm × 22 cm agar plate was placed in the middle of aluminum slab to establish a linear thermal gradient of 18–22° across the agar surface. In each assay, 15–20 young adult worms raised at 20° were washed in NGM buffer (ref) before being released in the middle of the agar surface (20°). Videos were captured using a CCD camera (Mightex Systems, BCE-B050-U) at 2 Hz for 20 min.

Whole genome sequencing

We sequenced *che-5*, *che-6* and *che-7* mutant animals, obtained from the CGC, with an Illumina GA2 genome analyzer. We used MAQGene for WGS data analysis (Bigelow *et al.* 2009). After subtraction of background variants found in two other sequenced *che* strains (*che-5*, *che-6* and *che-7*), we found six missense mutations on LGIV in the *che-6(e1126)*, where *che-6* had been previously mapped to (located in *inx-18*, C23H5.7, *gbb-2*, Y52D5A.2, *inx-7*, C46G7.3). No splice site or nonsense mutations were found. In the case of *che-7(e1128)* animals, we identified one nonsense and 22 missense mutations. In *che-5* mutants, we found 7 missense mutations on LGIV and tested available alleles of several candidates that failed to mimic the defective chemotaxis behavioral phenotype of *che-5*. We did not pursue this mutant further.

Heterologous expression and GC assays of GC proteins in tissue culture

GCY-4 and GCY-22 DNA fragments were synthesized in a human codon-optimized manner, and were subcloned, together with an FLAG epitope, into pcDNA3.1 expression vector. Constructs were transfected into CHO cells and the GC activity assay was performed as previously described (Guo *et al.* 2007, 2009). Cells were cultured in growth medium to ~95% confluency and were washed in a buffer containing 50 mM NH_4Ac and 200 mM sucrose pH 7 (plus 1 mM IBMX). Membrane preparations were made. 100 mM of NaCl, NaBr, $NaPO_4$, or NaI were used for treatment. After 20 min, the membrane preparations were lysed in 0.1 M HCl and assayed for cGMP concentration using Direct cGMP EIA Kits (NewEast Biosciences).

Results

Chimeric GCY receptor experiments demonstrate that specificity of rGC function lies in the extracellular domain

Figure 1B shows the general structure of receptor-type rGC proteins. They contain a large extracellular domain and many rGC proteins show similarity in this domain to small ligand binding bacterial proteins ("RFLBR domain" = receptor family ligand-binding region). On the intracellular side, rGC proteins contain a protein kinase-like domain and a cyclase domain. We chose to analyze the requirement of the extracellular and intracellular domain for the specific function of three different rGC proteins, GCY-1, GCY-4 and GCY-22. GCY-1 is expressed in ASER, not ASEL and is required for an efficient response to potassium ions, but not other ASER-sensed ions (Ortiz *et al.* 2006, 2009). GCY-4 is also expressed in ASER and is required for an efficient response to bromide and iodide ions, but not other ASER-sensed ions (Ortiz *et al.* 2006, 2009). GCY-22 is required for the processing of all ASER-sensed ions. Based on the previous suggestion that rGCs may form heterodimers (Morton 2004), we have proposed that GCY-22 may be a common subunit of the normally dimeric rGC proteins (Ortiz *et al.* 2009). As indicated in Figure 1C, we generated chimeric expression proteins in which the intra- and extracellular domains of all three proteins are swapped in all possible combinations. We generated stable transgenic lines that express each of these constructs, as well as wild-type controls, using the ASER-specific *gcy-5* promoter. We then crossed transgenic lines into *gcy-1*, *gcy-4*, and *gcy-22* mutant backgrounds to ask which of these constructs rescue the respective mutant phenotype.

We find that the potassium response defect in *gcy-1* mutant animals is rescued by *gcy-1*^{Extra}::*22* ^{Intra} (extracellular

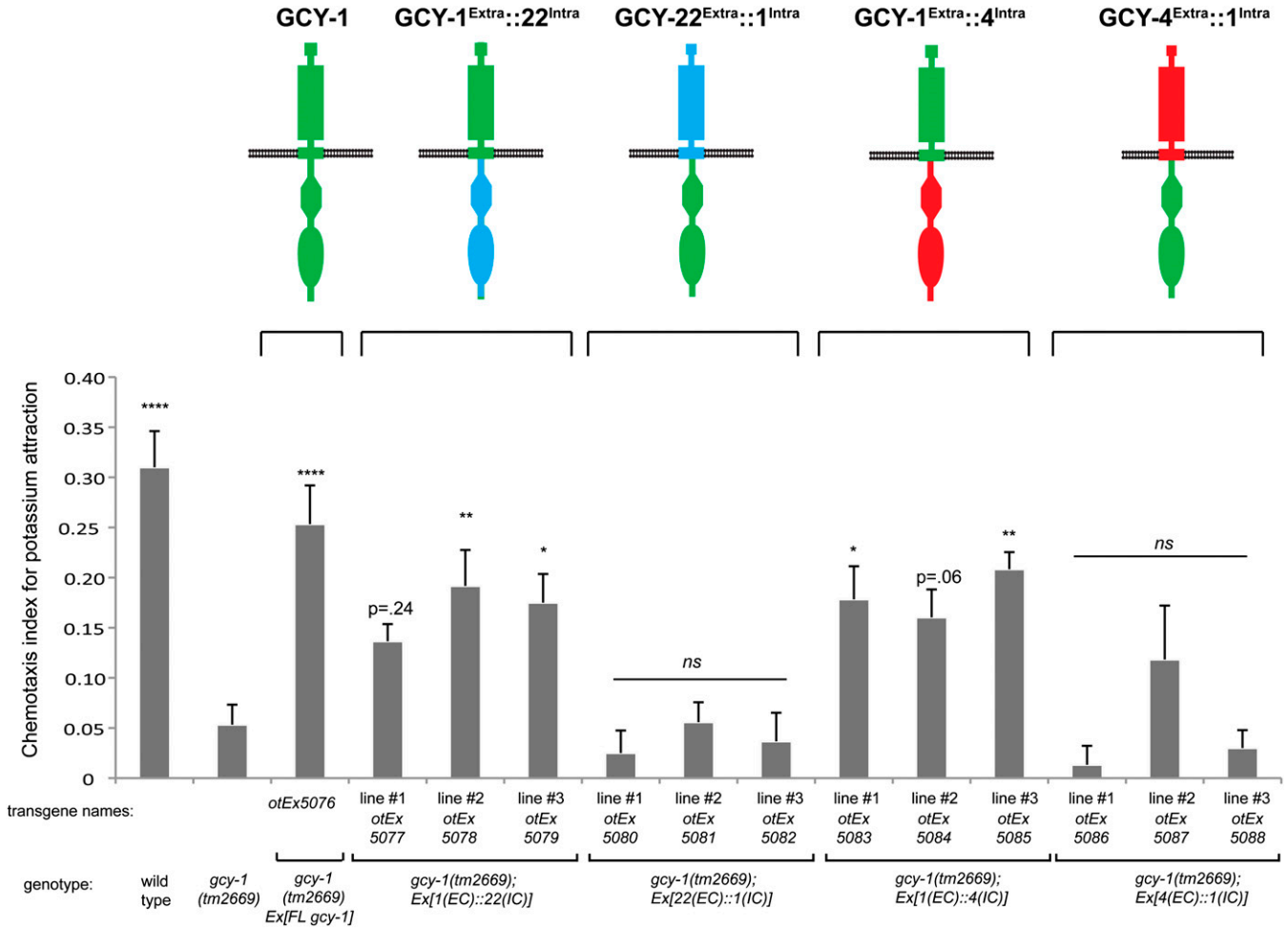

Figure 2 Chimera rescue experiments demonstrate the importance of the extracellular domain of GCY-1. Results of population salt chemotaxis assays are shown for wild-type, mutant, and transgenic strains. Three independent lines of receptor chimeras were tested for whether they can rescue *gcy-1* mutant defects. Analysis was completed using a one-way ANOVA with repeated measures comparing the mean of each group to the mean of the mutant *gcy-1*. Error bars indicate SEM. The Holm–Sidak correction was used to adjust for multiple comparisons and $\alpha = 0.1$. All *P*-values reported are the adjusted value after the correction was applied. *P*-values: $^{****}P < 0.0001$, $^{**}P < 0.01$, $^{*}P < 0.05$; NS, not significant ($P > 0.05$). $n = 6$ with each sample being a duplicate of two plates with four worms per plate. Assays were done blind to the genotype under test.

domain of GCY-1, intracellular domain of GCY-22) and by *gcy-1* ^{Extra}::*4* ^{Intra} chimeras (three extrachromosomal lines each; Figure 2). In contrast, the *gcy-1* defect is not rescued by *gcy-4* ^{Extra}::*1* ^{Intra} or by *gcy-22* ^{Extra}::*1* ^{Intra} chimeras (three extrachromosomal lines each; Figure 2). These results demonstrate that the specificity determinant of *gcy-1* function resides in the extracellular domain of the GCY-1 protein.

The same theme is readily apparent upon the analysis of iodide response defect in *gcy-4* mutant animals expressing various *gcy-4* chimeric constructs. The *gcy-4* defects are rescued by *gcy-4*^{Extra}::*22* ^{Intra} and by *gcy-4* ^{Extra}::*1* ^{Intra} chimeras (three extrachromosomal lines each; Figure 3). In contrast, no rescue is observed in *gcy-4* mutants expressing the *gcy-22* ^{Extra}::*1* ^{Intra} or by *gcy-22* ^{Extra}::*4* ^{Intra} chimeras (each three extrachromosomal lines; Figure 3).

Lastly, the chloride response defect of *gcy-22* mutant animals (only observed in *gcy-22*, but not *gcy-1* or *gcy-4* mutant animals) is rescued by *gcy-22*^{Extra}::*1* ^{Intra} and by *gcy-22*^{Extra}::*4* ^{Intra} chimeras, but not by *gcy-1* ^{Extra}::*22* ^{Intra} or by *gcy-4* ^{Extra}::*22* ^{Intra} chimeras (three extrachromosomal lines each; Figure 4A). This result is in accordance with all other chimera experiments, again showing that the specificity of rGC protein function resides in their extracellular domains.

In contrast to GCY-4 (involved in iodide response, but not potassium or chloride response) and GCY-1 (involved in potassium response, but not iodide or chloride response), GCY-22 is involved in the response to chloride, potassium and iodide (Ortiz *et al.* 2009). We therefore asked whether the involvement of GCY-22 in the iodide response is, like the response to chloride, dependent on the extracellular domain of GCY-22 or whether in this case, the extracellular domain of iodide-sensing GCY-4 could substitute for the extracellular domain of GCY-22. We find that it is again the extracellular domain of GCY-22 that is required to rescue the *gcy-22* mutant phenotype (Figure 4B). A chimera with the extracellular domain of GCY-4, even though required to rescue the

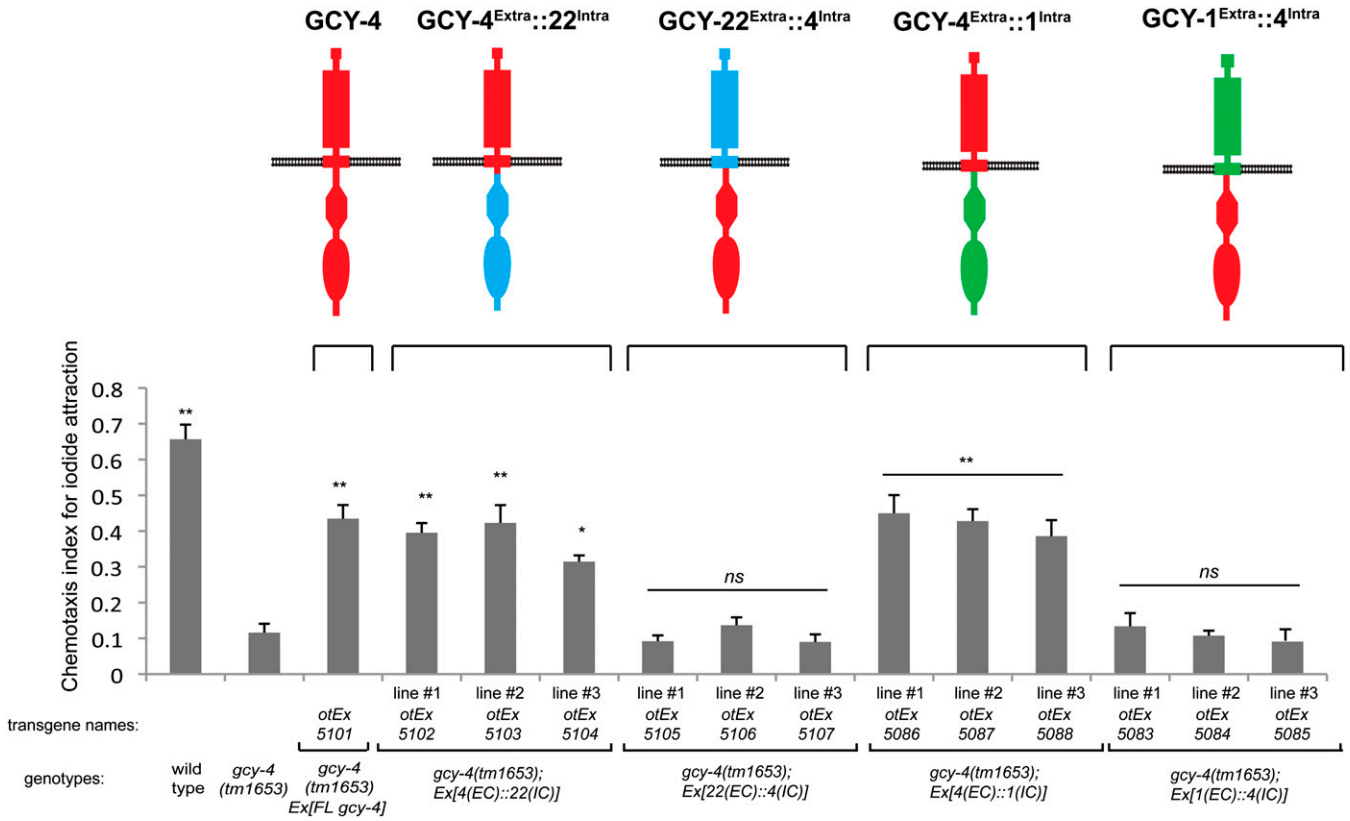

Figure 3 Chimera rescue experiments demonstrate the importance of the extracellular domain of GCY-4. Results of population salt chemotaxis assays are shown for wild-type, mutant, and transgenic strains. Three independent lines of receptor chimeras were tested for whether they can rescue *gcy-4* mutant defects. Analysis was completed using a one-way ANOVA with repeated measures comparing the mean of each group to the mean of the mutant *gcy-4*. Error bars indicate SEM. The Holm–Sidak correction was used to adjust for multiple comparisons and $\alpha = 0.05$. All *P*-values reported are the adjusted value after the correction was applied. *P*-values: $^{**}P < 0.0001$, $^{*}P < 0.001$; NS, not significant ($P > 0.01$). Error bars indicate SEM. $n = 6$ with each sample being a duplicate of two plates with four worms per plate. Assays were done blind to the genotype under test.

iodide defects of *gcy-4* mutants, is not able to substitute for GCY-22 function (Figure 4B).

GCY-4 and GCY-22 are sufficient to impose salt responsiveness onto other neuron types

If rGC proteins were indeed direct chemoreceptors, misexpression of rGC proteins in other neuron types should confer salt responsiveness to these neurons. To test this possibility, we pursued the following strategy. We used the *che-1* genetic mutant background in which the development and function of the ASE neurons is abrogated (Uchida *et al.* 2003; Etchberger *et al.* 2007). *che-1* mutant animals are unable to respond to salt cues (Figure 5). We then attempted to restore salt responsiveness by misexpressing rGC proteins in all other worm sensory neurons, using the *osm-6* promoter. Because of the absence of ASE (*che-1* mutant background), these animals will only be able to respond to salt cues if any other sensory neuron is now able to confer salt responsiveness. We chose specifically the *osm-6* promoter because it is active in all sensory neurons, including ASE (Collet *et al.* 1998), therefore allowing us to test through mutant rescue assays whether the expression construct indeed produces functional protein, as detailed below. We also anticipated that a broadly expressed promoter may hedge our bets to hit a neuron that could provide a functional response.

We used the GCY-4 protein, which is normally required for bromide and iodide response and the presumed common subunit GCY-22. We generated transgenic animals that express a chromosomally integrated *osm-6*^{prom}::*gcy-4* expression construct. We confirmed that this transgene produces functional protein by its ability to rescue the iodide response defect of *gcy-4* mutant animals (Figure 5A; note that this controls illustrates the usefulness of the *osm-6* promoter). We then transferred the array from the *gcy-4* mutant background into a *che-1* mutant background. *che-1*; *Is[osm-6*^{prom}::*gcy-4]* animals are unable to respond to bromide/iodide, suggesting that *gcy-4* alone is not sufficient to confer bromide/iodide responsiveness (Figure 5C). Similarly, we generated animals with an extrachromosomal array that contains a *osm-6*^{prom}::*gcy-22* expression construct. We confirmed that this transgene is able to rescue the iodide response defect of *gcy-22* mutant animals (Figure 5B) and then transferred the array from the *gcy-22* mutant background into the *che-1* background. Like *che-1*; *Is[osm-6*^{prom}::*gcy-4]* animals, *che-1*; *Ex[osm-6*^{prom}::*gcy-22]* animals

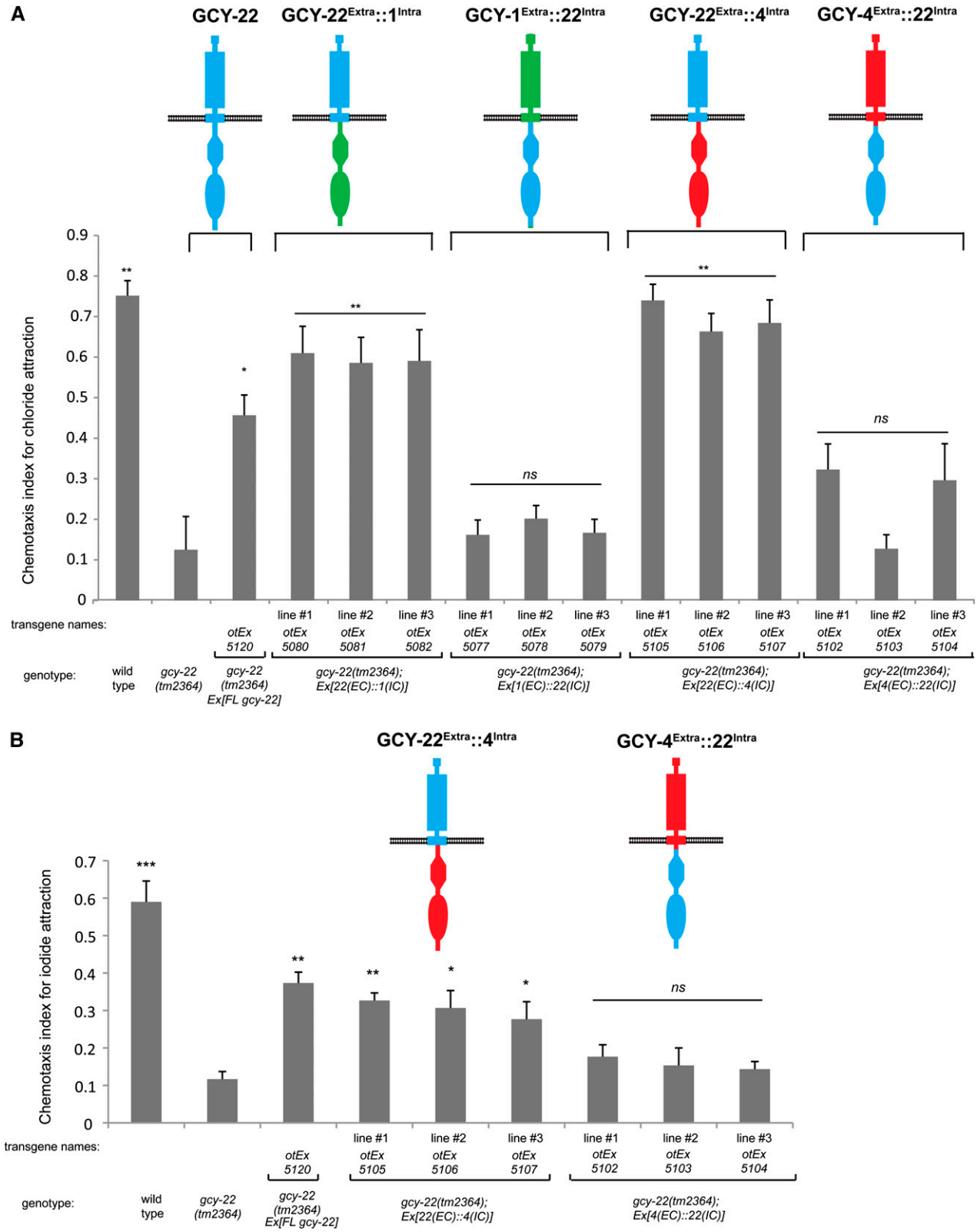

Figure 4 Chimera rescue experiments demonstrate the importance of the extracellular domain of GCY-22. Results of population salt chemotaxis assays are shown for wild-type, mutant, and transgenic strains. Three independent lines of receptor chimeras were tested for whether they can rescue gcy-22 mutant defects. For both A and B, error bars indicate SEM. Analysis was completed using a one-way ANOVA with repeated measures comparing the mean of each group to the mean of the gcy-22 mutant. Error bars indicate SEM. The Holm–Sidak correction was used to adjust for multiple comparisons and $\alpha = 0.05$. All P-values reported are the adjusted value after the correction was applied. (A) GCY-22 chimeras in chloride response. *P*-values:

are also not able to respond to iodide (Figure 5C). However, when we crossed the *Is[osm-6^{prom}::gcy-4]* and *Ex[osm-6^{prom}::gcy-22]* transgenes together, again in the context of a *che-1* mutant background, we find that the resulting double transgenic *che-1*; *Is[osm-6^{prom}::gcy-4]*; *Ex[osm-6^{prom}::gcy-22]* animals are able to respond to iodide (Figure 5C). These results demonstrate that *gcy-4*, in combination with *gcy-22*, is capable of imposing iodide responsiveness to other sensory neuron types and are consistent with the possibility that GCY-4/GCY-22 constitute a heteromeric iodide receptor complex. We can at present not exclude the possiblity that GCY-4 and GCY-22 cooperate in distinct neurons to impose a chemosensory response.

It is surprising that pansensory expression of GCY-4/GCY-22 with the *osm-6* driver permits salt attraction since the activation of a number of sensory neurons (*e.g.*, AWB, ASH or ADL) are thought to mediate repulsive behavior (Bargmann 2006). Perhaps any potential repulsive response of these neurons is overwhelmed by the expression of GCY-4/22 in attractive neurons. Also, GCY-4/22 may only be appropriately transported in some but not other neurons.

To further pursue reconstitutation experiments, but now in a more cell-type specific manner, we expressed GCY-4 and GCY-22 alone and in combination in the ASI sensory neurons, using the *srg-47^{prom}* driver. The ASI neurons have sensory ending that, like, for example the gustatory ASE and ASG neurons, are exposed to the environment and sense a variety of distinct stimuli (Bargmann 2006). The *gcy-4* and *gcy-22* transgenes were expressed in a *che-1* mutant background to ask whether the loss of ASE-mediated iodide attraction can rescue the ASI-expression of GCY-4/GCY-22. We find that *srg-47^{prom}::gcy-4* or *srg-47^{prom}::gcy-22* alone does not provide substantial rescue of the iodide attraction phenotype of *che-1* mutants, but coexpression of *srg-47^{prom}::gcy-4* and *srg-47^{prom}::gcy-22* does provide significant rescue (Figure 5D). A conceptually similar reconstitution experiment in the AWC olfactory neurons resulted in no rescue, consistent with the fact that the AWC dendritic endings are not exposed to the environment (data not shown). Taken together, the ASI-specific reconstitution experiment provides further support for the hypothesis that GCY-4 and GCY-22 may collaborate, possibly as a heterodimer, to confer a chemosensory function.

Lastly, we attempted to measure salt-inducible GCY protein activity in heterologous cell culture aassys (Guo *et al.* 2007, 2009). We co-expressed GCY-4 and GCY-22 proteins in Chinese hamster ovary (CHO) cells and tested whether guanylyl cyclase activity could be directly stimulated by bromide, chloride, or sodium. No significant stimulations were observed (Figure S1), but given the negative nature of these results, they cannot rule out that GCY-4/GCY-22 constitute a bromide/iodide receptor complex.

In conclusion, pansensory GCY-4/GCY-22 expression is able to restore iodide attraction of animals that contain no functional ASE neuron, which supports, but does not ultimately prove the notion that GCY-4/GCY-22 form a functional iodide receptor.

che-6 is a cyclic nucleotide gated ion channel likely acting as an effector of rGC proteins in the ASE neurons

To identify additional molecules involved in rGC-mediated gustatory signal transduction in the ASE neurons, we determined the molecular identity of two as yet uncloned chemotaxis (*che*) mutants, *che-6* and *che-7*, using whole genome sequencing (WGS). *che-6* and *che-7* were isolated in screens for mutants unable to respond to sodium and chloride ions (Lewis and Hodgkin 1977) but have not since been further analyzed. We find that *che-7* mutant animals carry a mutation in *inx-4*, which codes for a gap junction component broadly expressed in the nervous system (Figure 6, A–C). Based on its molecular identity and expression pattern (several head neurons, but not ASE; Altun *et al.* 2009), this gene likely acts downstream of primary signal transduction events and we did not pursue its characterization any further. In contrast, we find *che-6* to indeed code for another gustatory signaling component and we therefore chose to focus on the characterization of *che-6*.

Specifically, we found through WGS that the previously identified *che-6(e1126)IV* strain bears mutations in six different coding loci on chromosome IV, one of them a mutation in the previously uncharacterized *cng-4/C23H5.7* gene (*Materiala and Methods*; Figure 7, A and B), which encodes a predicted cyclic nucleotide-gated ion channel. The *e1126* mutation is a missense mutation in the nucleotide-binding domain (Figure 7, A and B). The chemotaxis defect of *che-6 (e1126)IV* can be rescued by supplying a piece of genomic DNA that contains the wild-type copy of the *cng-4* locus (Figure 8A). Animals carrying a deletion allele, *tm5036*, that removes the critical cyclic nucleotide-binding domain of the *cng-4* gene, kindly provided by Shohei Mitani and the National Bioresource Project of Japan, show the same phenotype as the *che-6(e1126)* mutant animals (Figure 8A). From here on we refer to *cng-4* as *che-6*.

The *C. elegans* genome codes for a total of six predicted CNG channels (Kaupp and Seifert 2002). Sequence analysis indicates that one of them, *tax-4*, is a homolog of the α-type subunit of CNGs, while another one, *tax-2*, is a β-type subunit (Figure 7C) (Kaupp and Seifert 2002). Both *tax-2* and *tax-4* have been extensively characterized in terms of function and expression (Coburn and Bargmann 1996; Komatsu *et al.* 1996). The four remaining CNGs are more divergent but have a somewhat greater overall sequence similarity to the α-type, based on the sequence comparison of the entire proteins or individual domains (Figure 7C; Figure S2). However, only two

$^{**}P < 0.0001$, $^{*}P < 0.001$; NS, not significant ($P > 0.01$). n = 6 with each sample being the average of the duplicate of two plates with four worms per plate. (B) GCY-22 chimeras in iodide response. *P*-values: $^{**}P < 0.0001$, $^{**}P < 0.01$, $^{*}P < 0.05$; NS, not significant ($P > 0.05$). $n = 3$ with each sample being the average of the duplicate of two plates with four worms per plate.

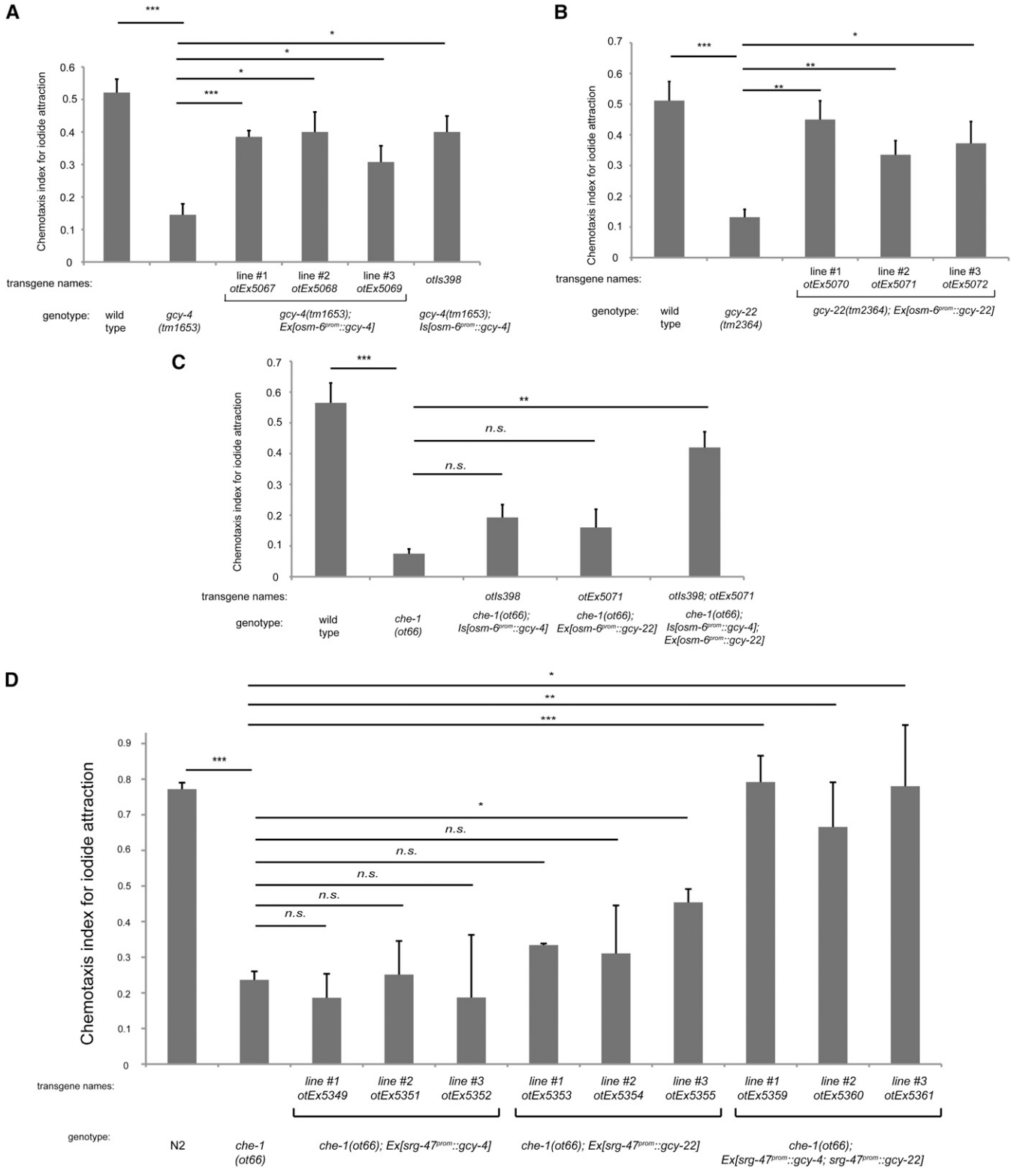

Figure 5 Ectopic expression of *gcy-4* and *gcy-22* confers iodide responsiveness on ASE-deficient animals. (A) Pansensory expression of *gcy-4* rescues the *gcy-4* mutant phenotype, as observed with the independent extrachromosomal arrays expressing *osm-6*^{prom}*::gcy-4* and one chromosomal integrant generated from one of the extrachromosomal arrays. (B) Pansensory expression of *gcy-22* rescues the *gcy-22* mutant phenotype, as observed with the independent extrachromosomal arrays expressing *osm-6*^{prom}*::gcy-22*. Panel A and B are control experiments that establish the functionality of the individual transgenes. (C) A transgenic strain that expresses the integrated *osm-6*^{prom}*::gcy-4* array from A or one extrachromosomal *osm-6*^{prom}*::gcy-22* array is not able to rescue the loss of ASE neuron functionally (*che-1* mutant background in which ASE fail to differentiate and do not express *gcy-4* or *gcy-22*). However, combining the *osm-6*^{prom}*::gcy-4* integrated array with the *osm-6*^{prom}*::gcy-22* extrachromosomal array results in rescue of the *che-1*

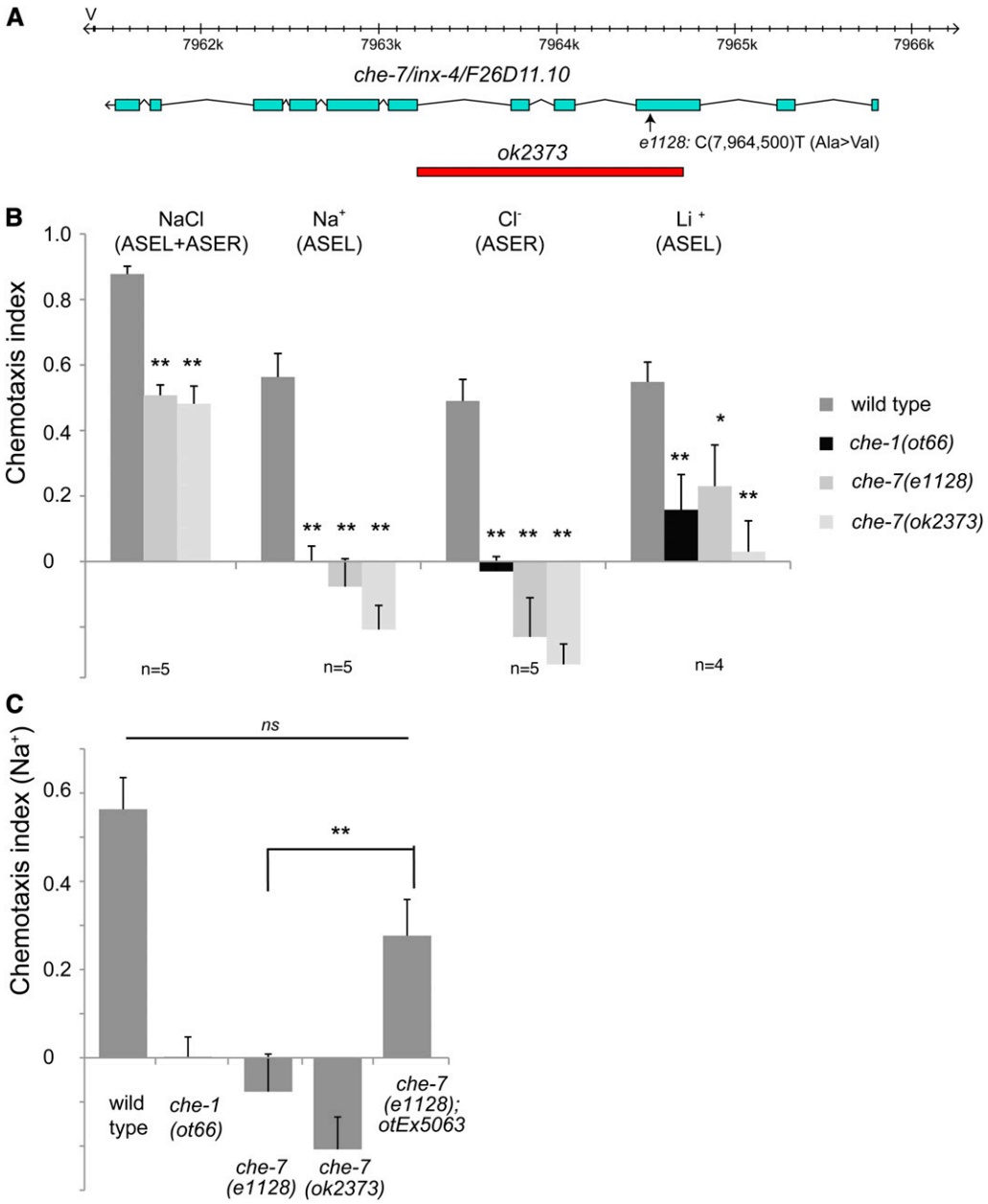

Figure 6 *che-7* corresponds to the *inx-4* gene. Three lines of evidence for *che-7* being *inx-4* are shown here, one for each panel. (A) *che-7(e1128)* animals carry a mutation in the *inx-4* gene (Ala→Val at 7964500) within the third exon. The missense mutation lies within the third transmembrane domain. (B) Chemotaxis defects of *che-7(e1128)* animals are similar to those of *inx-4(ok2373)* animals. The assay used here is a population assay. Each *n* shown in the figure is the average of two assays done in duplicate on the same day and each assay has between 50 and 250 worms. Statistics were measured using unpaired Student's *t*-test assuming equal variance and the Bonferroni correction was used to adjust the *P*-values. Error bars indicate the SEM. *P*-values: $^{**}P < 0.01$, $^{*}P < 0.05$; NS, not significant ($P > 0.05$). (C) The *che-7* chemotaxis defect can be rescued with a fosmid (WRM0620bH04) covering the *inx-4* locus, contained on the *otEx5063* array. $n = 5$ with each sample being a duplicate of two plates with four worms per plate. Statistics were measured using unpaired Student's *t*-test assuming equal variance and the Bonferroni correction was used to adjust the *P*-values. Error bars indicate the SEM. *P*-values: $^{**}P < 0.01$, $^{*}P < 0.05$; NS, not significant ($P > 0.05$).

of the four proteins, CNG-1 and CNG-3, contain a negatively charged amino acid in the ion-conducting pore, which is a characteristic feature of α-subunits. Three of them, CNG-1, CNG-2, and CNG-3, contain leucines in their extreme C termini that are predicted to form coiled coils, another defining feature of α-subunits. Whether any of these four proteins fulfill the classic definition of an α-subunit of being able to assemble ion-conducting channels on their own, remains to be shown.

Deletion alleles of two of the four divergent CNGs, *cng-1* and *cng-3*, have been functionally characterized previously, showing no defects in salt chemotaxis and olfaction, respectively (Cho *et al.* 2004, 2005). The remaining two CNGs,

mutant phenotype (last bar). (D) ASI-specific expression of *GCY-4* and *GCY-22* compensates for loss of *che-1*. Three lines that coexpress *srg-47*^{prom}::*gcy-4* and *srg-47*^{prom}::*gcy-22* arrays are able to rescue the chemotaxis defect of *che-1* mutants to iodide. In all panels, error bars indicate the SEM. Analysis was completed using a one-way ANOVA with repeated measures comparing the mean of each group to the mean of the mutant. Error bars indicate SEM. The Holm–Sidak correction was used to adjust for multiple comparisons and a = 0.01. All *P*-values reported are the adjusted value after the correction was applied. *P*-values: $^{***}P < 0.001$, $^{**}P < 0.01$, $^{*}P < 0.05$; NS, not significant ($P < 0.05$). In A–C, n = 4 and in D, n = 3 with each sample being the average of the duplicate of two plates with four worms per plate. Assays were done blind to the genotype under test.

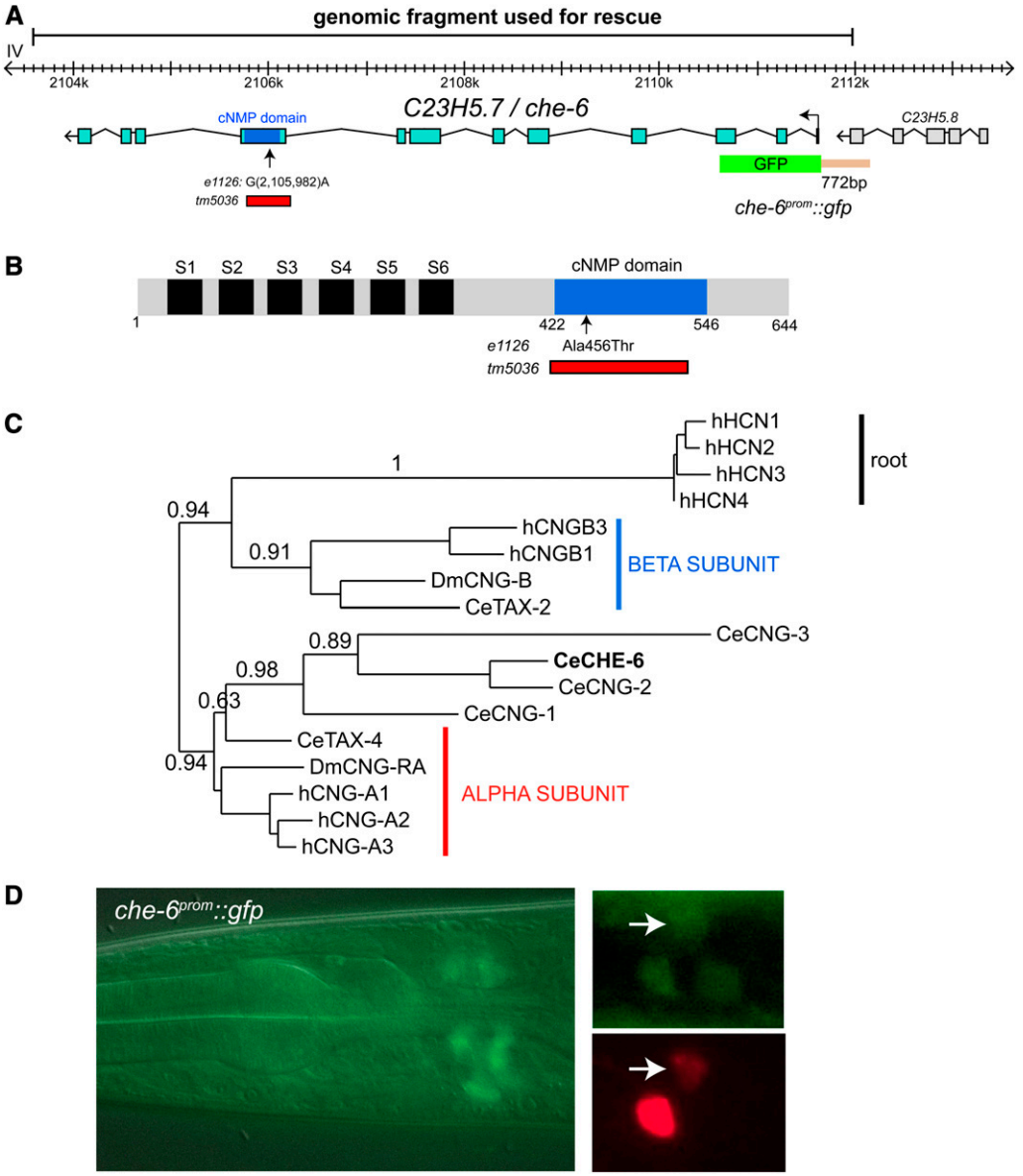

Figure 7 *che-6* codes for a cyclic nucleotide-gated ion channel. (A) *che-6* gene structure and alleles. The alanine-encoding codon mutated in *e1126* to a threonine-encoding codon resides in the nucleotide-binding domain. Generally, within nucleotide-binding domains, this position is either an alanine or a glycine (Kaupp and Seifert 2002). (B) Schematic protein structure of *CHE-6*s. (C) Phylogenetic tree built at the www.phylogeny.fr suite (Dereeper *et al.* 2008). Full-length protein sequence was used an Hyperpolarization-activated cyclic nucleotide-gated channel (HCN; no worm homologs) were used to root the tree. A similar clustering is observed if only the cNMP domain or the ion channel domain is used (Figure S2). (D) *che-6*^{prom}*::gfp* expression pattern. The left panels show the overview of expression in several adult head neurons. The two smaller panels on the right show an image of the head region of a transgenic animal coexpressing *che-6*^{prom}*::gfp (hanEx24)* and ASE + AWC-expressed *ceh-36*::*mCherry (otIs264)*, revealing overlap of expression in ASE and AWC.

cng-2 and *che-6* (previously called *cng-4*), have not been functionally characterized to date.

che-6 is expressed and functions in ASE

Sensory neuron-specific expression profiles in subsets of amphid neuron pairs have previously been described for *tax-2*, *tax-4*, *cng-1*, and *cng-3* (Coburn and Bargmann 1996; Komatsu *et al.* 1996; Cho *et al.* 2004, 2005), but not for *cng-4/che-6*. We generated a *che-6* reporter gene fusion that contains 722 nucleotides upstream of the start codon and that encompasses all intergenic sequences to the next upstream gene (schematically shown in Figure 7A). This intergenic region contains a putative *cis*-regulatory motif, the "ASE motif" (GAAGCC), which is found in many genes expressed in the ASE neurons and is a binding site for the terminal selector transcription factor *che-1* (Etchberger *et al.* 2007). We found that this reporter is expressed weakly in approximately five neuron pairs, one of them the ASE neuron pair (Figure 7D).

To corroborate the cellular focus of *che-6* action, we expressed the *che-6* locus in *che-6* mutant animals under control of the *ceh-36* promoter, which is active in the ASE gustatory neurons and the AWC olfactory neurons (Lanjuin *et al.* 2003). We find that two out of three lines show rescue of the *che-6* mutant chemotaxis phenotype (Figure 8B), indicating that *che-6* acts in the ASE neurons to control chemosensory behavior.

che-6 affects gustatory, but not olfactory or thermosensory behavior, and cng-3 affects thermosensory behavior

We tested the effect of loss of *che-6* on additional sensory modalities. We examined salt chemotaxis, which is primarily mediated by the ASE neurons [as done previously by Lewis

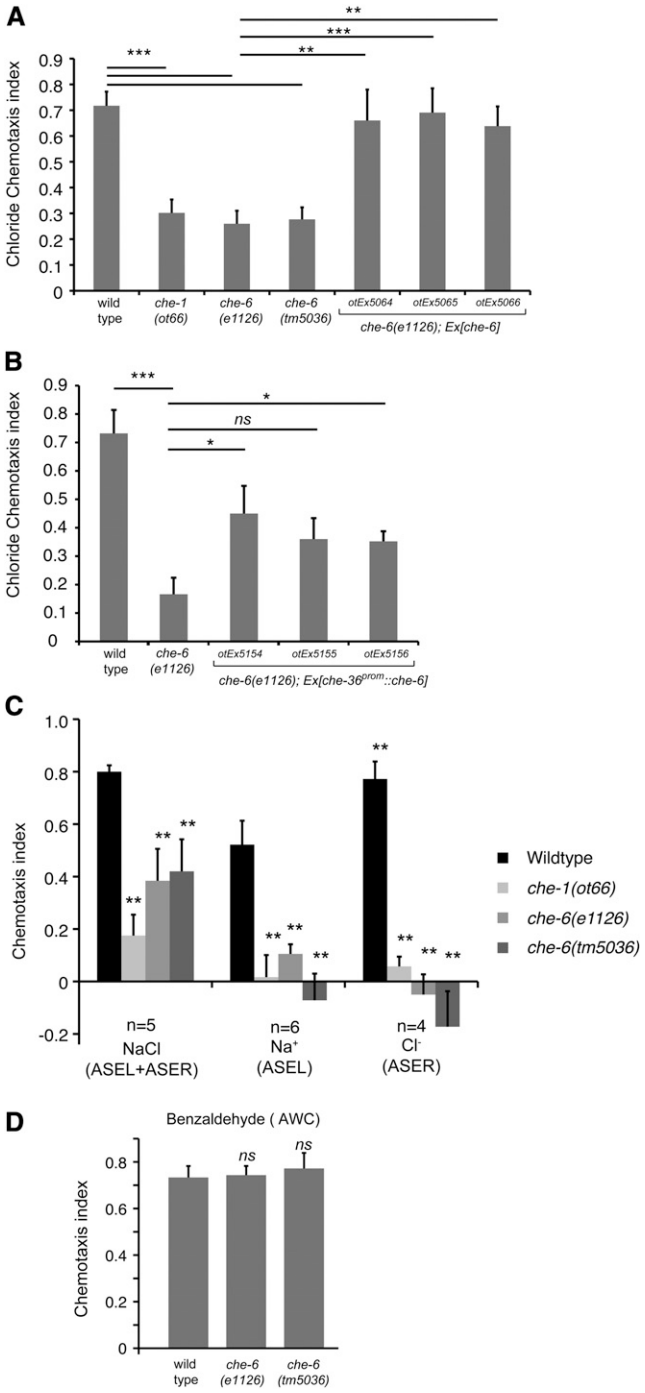

Figure 8 Chemotaxis defects of *che-6* mutant animals. (A) Two different *che-6* alleles show similar chemotaxis defects as observed upon loss of the ASE neurons (*che-1* mutants (Uchida *et al.* 2003) and transformation rescue of the *che-6* mutant phenotype with a piece of genomic DNA illustrated in Figure 7A. Error bars indicate SEM. Analysis was completed using a one-way ANOVA comparing the mean of each group to the mean of the mutant *che-6 (e1126)*. The Holm–Sidak correction was used to adjust for multiple comparisons and $\alpha = 0.01$. All *P*-values reported are the adjusted value after the correction was applied. *P*-values: $***P < 0.001$, $**P < 0.01$, $*P < 0.05$; NS, not significant ($P > 0.05$). n = 4–13 replicates with each n being the average of the duplicate of two plates with four worms per plate. (B) Rescue of the *che-6* mutant phenotype with a transgene that expresses *che-6* under control of the *ceh-36* promoter in ASE and AWC. $n = 5$ with each sample being the average of the a duplicate of two plates with four worms per plate. (C) *che-6* mutants fail to respond to ASEL and ASER-sensed cues. The assay used here is a population assay. n = 3–5 and each n shown in the figure is an average of two assay plates done in duplicate on the same day with between 50 and 250 worms per plate. (D) *che-6* mutants show a normal response to the AWC-sensed olfactory cue benzaldehyde. The assay used here is a population assay. $n = 3$ with each n being the average of two assay plates done in duplicate on the same day with between 50 and 250 worms per plate. For B and D, statistics were measured using unpaired Student's *t*-test assuming equal variance comparing the mean of each group to the mean of the mutant *che-6 (e1126)* and the Bonferroni correction was used to adjust the *P*-values. Error bars indicate the SEM. *P*-values: $**P < 0.01$, $*P < 0.05$; NS, not significant ($P > 0.05$).

and Hodgkin (1977), but now done with different assays], thermotaxis primarily mediated by the AFD thermosensory neurons (Mori and Ohshima 1995) and olfactory attraction mediated by the AWC sensory neurons (Bargmann *et al.* 1993). We confirmed that *che-6* mutant animals are defective in salt chemotaxis as determined by our chemotaxis assay system (Figure 8C). Salt chemotaxis defects extend to ions sensed by either ASEL (sodium) or ASER (chloride) (Figure 8C). However, we found that *che-6* mutants show no defects in AWC-mediated olfactory behavior (Figure 8D) and no defects in thermotaxis behavior (Figure 9; Figure S3).

While we observed no thermotaxis defects in *che-6* mutants, we observed thermotaxis defects in animals lacking the *cng-3* gene (Figure 9; Figure S3), which was previously shown to be expressed in the AFD thermosensory neurons (Cho *et al.* 2004). Since *tax-2* and *tax-4* channels also show defects in both thermotaxis and salt chemotaxis (Komatsu *et al.* 1996) (Figure 9; Figure S3), these findings suggest that *che-6* and *cng-3* form sensory modality-specific subunits with the more broadly acting *tax-2* and *tax-4* (see *Discussion*).

Discussion

Mechanisms of salt sensation: the rGC proteins

In combination with our previous work (Ortiz *et al.* 2009), this work has provided genetic evidence in support of the notion that rGC proteins may work as direct receptors for salt ions. We have shown previously through genetic loss-of-function analysis that individual *gcy* genes are required for the efficient response of animals to specific salt ions, both on the level of behavior as well as neuronal activity (Ortiz *et al.* 2009). We have extended these observations here by showing (a) that the ion-selectivity in rGC protein function lies in their extracellular domain and (b) that rGC proteins can confer salt responsiveness to other sensory neurons.

GCY-1 and GCY-4 may operate as direct sensors of potassium and iodide, respectively. GCY-22 may operate as a direct sensor of chloride. The involvement of GCY-22 in iodide and potassium sensation, for which the extracellular domain is again essential, may lie in GCY-22 being a common subunit for the usually hetero- or homodimeric rGC proteins, as previously speculated (Ortiz *et al.* 2009). That is, GCY-22

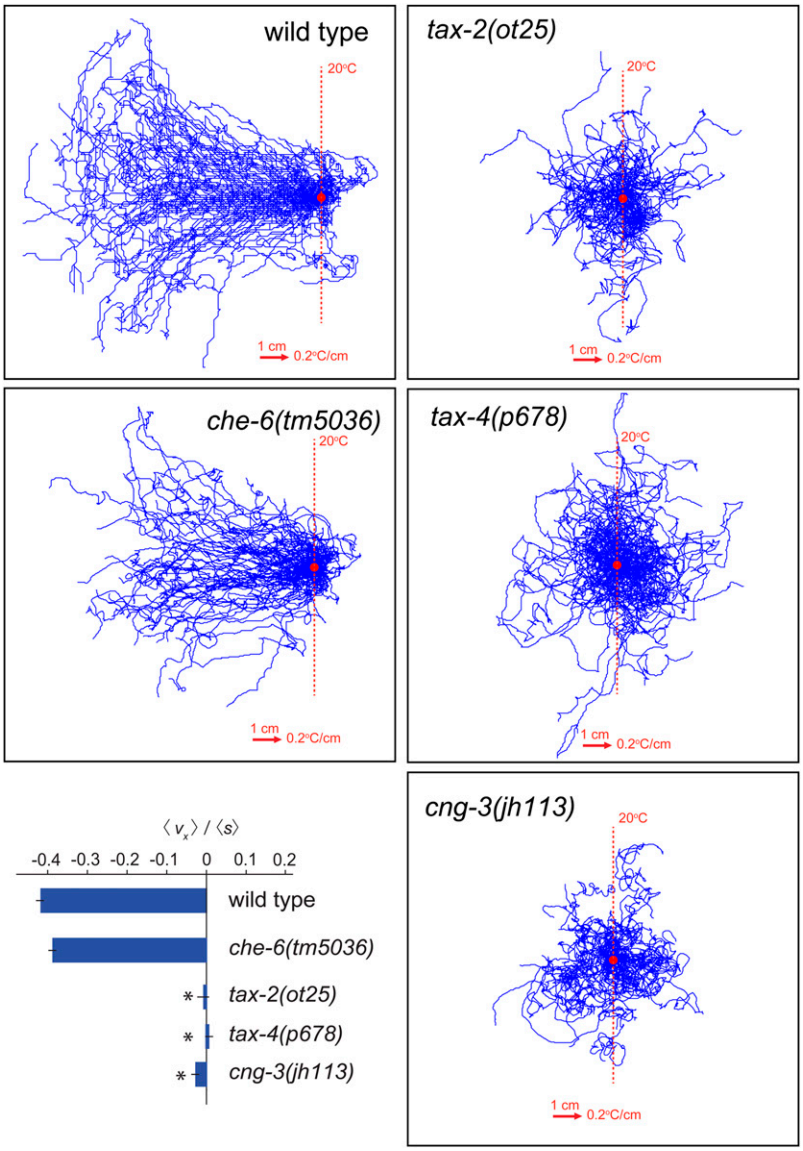

Figure 9 Thermotaxis behavior of the CNG channel mutants *che-6* and *cng-3*. Representative trajectories and navigational indexes (boxed inset) of wild-type N2 (n = 100), *che-6(tm5036)* (n = 60), *tax-2(ot25)* (n = 60), *tax-4 (p678)* (n = 60), and *cng-3(jh113)* (n = 40) animals navigating linear spatial thermal gradients (0.2°/cm) on the surface of 22 cm × 22 cm plates. Worms grown at 15° were started at 20°. Trajectories were aligned to have the same starting point for presentation purposes. Navigational indexes are defined as $\langle v_g \rangle / \langle s \rangle$. $\langle v_g \rangle$ indicates the mean velocity in the direction up the gradient. $\langle s \rangle$ indicates crawling speed along trajectories. An alternative data representation is shown in Figure S3.

may form a heterodimeric iodide receptor with GCY-4, a heterodimeric potassium receptor with GCY-1 and it may form a heterodimeric chloride receptor with an as yet uncharacterized GCY subunit. Since none of the other presently known ASE-expressed GCY proteins are involved in chloride chemotaxis, it is also conceivable that GCY-22 may constitute a homodimeric chloride receptor on its own. It is important to point out that a heterodimeric constitution of rGCs protein still awaits biochemical proof and that our genetic data are nothing more than consistent with such a hypothetical model.

A receptor function of rGCs, rather than a more intermediary, signal-transducing role, is also consistent with the notion that gustatory sensory transduction in the ASE neurons appears independent of GPCR signaling in which rGCs are normally embedded in as signaling intermediates (Bargmann 2006). A GPCR-coupling of rGCs is unlikely in ASE neurons since ASE-mediated chemosensation is independent of all characterized heterotrimeric G proteins (Jansen *et al.* 1999, 2002), is independent of the GPCR-regulatory kinase GRK-2 (Fukuto *et al.* 2004), and is independent of the ODR-4/ODR-8 GPCR trafficking system (Dwyer *et al.* 1998).

There are other rGCs that may operate as direct sensory receptors. Based on genetic loss-of-function analysis, the three rGC proteins GCY-8, GCY-18, and GCY -23 are candidate thermosensors in the AFD thermosensory neurons (Inada *et al.* 2006; Ramot *et al.* 2008; Wasserman *et al.* 2011) and GCY-9 is a candidate carbon dioxide receptor (Hallem *et al.* 2011; Brandt *et al.* 2012). In none of these cases, however, has it been tested whether the extracellular domains are dispensable for function, as it is the case for an rGC, ODR-1, in olfactory signal transduction (L'Etoile and Bargmann 2000) or whether the extracellular domains are required for function, as we show here for the gustatory rGCs. A direct receptor function of rGC proteins would also be reminiscent of the function of soluble GCs (sGCs) as

direct sensory receptors for another ambient cue, oxygen. In this case, the ligand sensor domain is a heme binding domain (Gray *et al.* 2004; Cheung *et al.* 2005). Ligand binding activates the cyclase resulting in cGMP production that in turn activates the TAX-2/TAX-4 CNG complex in oxygen-sensing neurons.

Biochemical studies showing that changes in salt concentration can activate cyclase activity of the rGC proteins in a heterologous *in vitro* system would be the ultimate proof for receptor function, but our attempts to detect sensory stimulus-induced activation have so far not been successful. There are also no reports of *in vitro* activation of other candidate rGC sensory receptors through defined sensory stimuli (such as the GCY-8, -9, -18, -23 proteins mentioned above). Our failure to detect salt-stimulated activity *in vitro* could be the result of several different complications associated with correct expression, localization, and folding of *C. elegans* proteins in vertebrate cell culture or the absence of accessory subunits. In the absence of such biochemical data, alternative scenarios for rGC function cannot be excluded. For example, the extracellular domain of individual ASE-expressed GCY proteins may not itself be involved in salt sensation, but may be required to couple to the extracellular domain of other, specific salt-sensing proteins. Our GCY-4/GCY-22 reconstitution experiments could be explained by such specific salt sensor being expressed, but not normally functioning, in other sensory neurons. However, such a model seems less parsimonious than a direct role of rGC proteins in salt sensation.

A role for rGCs as direct sensory receptors should also be viewed from the perspective of the expansion of rGCs in nematode genomes (27 genes in *C. elegans vs.* 5 in humans), their apparent sequence diversity in different nematodes, and their predominant expression in sensory neurons (at least 25 out of 27 rGC-encoding genes are expressed in sensory neurons) (Ortiz *et al.* 2006). Species-specific expansions and diversification are general features of sensory receptor gene families (consider, for example, GPCR-type odorant receptors) and provide a reflection of the highly diverse and species-specific sensory environments that different organisms find themselves in. It will be interesting to determine the spectrum of sensory cues for other rGC proteins.

Mechanisms of salt-triggered signal transduction: the CNG channels

A nodal point in signal transduction in the ASE neurons is the cGMP-triggered gating of ion channels of the CNG family. Two CNGs acting in salt transduction in ASE were previously identified, TAX-2 (a β-subunit) and TAX-4 (an α-subunit) (Coburn and Bargmann 1996; Komatsu *et al.* 1996) and we have identified here a third CNG acting in ASE-mediated salt transduction, CHE-6. CNGs are known to be tetrameric channels composed of multiple distinct types of subunits (Kaupp and Seifert 2002). In rat olfactory neurons, tetrameric CNG channels are composed of three distinct subunits (Bonigk *et al.* 1999). Based on this precedent, we propose that the CNG channel in the ASE neurons is composed of TAX-2, TAX-4, and CHE-6 subunits.

Our genetic analysis suggests that CNG channels assemble and transduce signals in a cell-type specific manner. ASE-mediated salt sensation requires *tax-2*, *tax-4*, and *che-6*, but not *cng-3*. AFD-mediated thermosensory transduction requires *tax-2* and *tax-4* (Coburn and Bargmann 1996; Komatsu *et al.* 1996), but not *che-6* (this article). Instead, *cng-3* is required for efficient thermotaxis (this article). CNG channels may therefore have sensory- and cell-type specific compositions, with a CHE-6/TAX-4/TAX-2 channel in ASE and a CNG-3/TAX-4/TAX-2 channel in AFD. The olfactory AWC neurons also require TAX-2 and TAX-4 (Coburn and Bargmann 1996; Komatsu *et al.* 1996), but neither *che-6* (this article) nor *cng-3* (Cho *et al.* 2004); these neurons may employ a yet different CNG subunit, perhaps the as yet uncharacterized CNG-2 protein. Sensory neuron-type specific subunit compositions have also been described in vertebrates (Kaupp and Seifert 2002).

In conclusion, our studies have deepened our understanding of salt-induced sensory transduction, providing support for the hypothesis of rGC proteins functioning as direct salt receptors and identifying a key effector component of rGC-triggered signal transduction.

Acknowledgments

We thank Alex Boyanov for running our whole genome sequencing (WGS) operations, Richard J. Poole for the WGS data analysis, Qi Chen for generating transgenic strains, Kelly Howell for help with transgenic lines, Piali Sengupta and Yuichi Iino for helpful comments on the manuscript, Piali Sengupta for the *srg-47* promoter, the *Caenorhabditis* Genetics Center for providing the *che* strains, Shohei Mitani at Tokyo Women's Medical University School of Medicine for kindly providing the *che-6(tm5036)* allele, and the Vancouver/Oklahoma *Caenorhabditis elegans* knockout consortium directed by Don Moerman for the *che-7(ok2373)* allele. This work was funded by the National Institutes of Health (NIH) (R01NS050266 to O.H. and R01GM084191 to X.-Y.H.), an NIH pioneer award (A.D.T.S.), the National Science Foundation (A.D.T.S.), and the Howard Hughes Medical Institute (O.H.).

Literature Cited

Altun, Z. F., B. Chen, Z. W. Wang, and D. H. Hall, 2009 High resolution map of Caenorhabditis elegans gap junction proteins. Dev. Dyn. 238: 1936–1950.

Bargmann, C. I., 2006 Chemosensation in C. elegans (Oct. 25, 2006), WormBook, ed. The C. elegans Research Community, WormBook, PMID: 18050433/wormbook. http://www.wormbook.org.

Bargmann, C. I., and H. R. Horvitz, 1991 Chemosensory neurons with overlapping functions direct chemotaxis to multiple chemicals in C. elegans. Neuron 7: 729–742.

Bargmann, C. I., E. Hartwieg, and H. R. Horvitz, 1993 Odorant-selective genes and neurons mediate olfaction in C. elegans. Cell 74: 515–527.

Bigelow, H., M. Doitsidou, S. Sarin, and O. Hobert, 2009 MAQGene: software to facilitate C. elegans mutant genome sequence analysis. Nat. Methods 6: 549.

Birnby, D. A., E. M. Link, J. J. Vowels, H. Tian, P. L. Colacurcio *et al.*, 2000 A transmembrane guanylyl cyclase (DAF-11) and Hsp90 (DAF-21) regulate a common set of chemosensory behaviors in *Caenorhabditis elegans*. Genetics 155: 85–104.

Bonigk, W., J. Bradley, F. Muller, F. Sesti, I. Boekhoff *et al.*, 1999 The native rat olfactory cyclic nucleotide-gated channel is composed of three distinct subunits. J. Neurosci. 19: 5332–5347.

Brandt, J. P., S. Aziz-Zaman, V. Juozaityte, L. A. Martinez-Velazquez, J. G. Petersen *et al.*, 2012 A single gene target of an ETS-family transcription factor determines neuronal CO2-chemosensitivity. PLoS ONE 7: e34014.

Chang, S., R. J. Johnston, C. Frokjaer-Jensen, S. Lockery, and O. Hobert, 2004 MicroRNAs act sequentially and asymmetrically to control chemosensory laterality in the nematode. Nature 430: 785–789.

Chandrashekar, N., and S. D. Roper, 2010 The cell biology of taste. J. Cell Biol. (PMID 20107438)

Cheung, B. H., F. Arellano-Carbajal, I. Rybicki, and M. de Bono, 2004 Soluble guanylate cyclases act in neurons exposed to the body fluid to promote C. elegans aggregation behavior. Curr. Biol. 14: 1105–1111.

Cheung, B. H., M. Cohen, C. Rogers, O. Albayram, and M. de Bono, 2005 Experience-dependent modulation of C. elegans behavior by ambient oxygen. Curr. Biol. 15: 905–917.

Cho, S. W., K. Y. Choi, and C. S. Park, 2004 A new putative cyclic nucleotide-gated channel gene, cng-3, is critical for thermotolerance in Caenorhabditis elegans. Biochem. Biophys. Res. Commun. 325: 525–531.

Cho, S. W., J. H. Cho, H. O. Song, and C. S. Park, 2005 Identification and characterization of a putative cyclic nucleotide-gated channel, CNG-1, in C. elegans. Mol. Cells 19: 149–154.

Coburn, C. M., and C. I. Bargmann, 1996 A putative cyclic nucleotide-gated channel is required for sensory development and function in C. elegans. Neuron 17: 695–706.

Collet, J., C. A. Spike, E. A. Lundquist, J. E. Shaw, and R. K. Herman, 1998 Analysis of osm-6, a gene that affects sensory cilium structure and sensory neuron function in *Caenorhabditis elegans*. Genetics 148: 187–200.

Daniels, S. A., M. Ailion, J. H. Thomas, and P. Sengupta, 2000 egl-4 acts through a transforming growth factor-beta/SMAD pathway in caenorhabditis elegans to regulate multiple neuronal circuits in response to sensory cues. Genetics 156: 123–141.

Dereeper, A., V. Guignon, G. Blanc, S. Audic, S. Buffet *et al.*, 2008 Phylogeny.fr: robust phylogenetic analysis for the non-specialist. Nucleic Acids Res. 36: W465–W469.

Dusenbery, D. B., R. E. Sheridan, and R. L. Russell, 1975 Chemotaxis-defective mutants of the nematode *Caenorhabditis elegans*. Genetics 80: 297–309.

Dwyer, N. D., E. R. Troemel, P. Sengupta, and C. I. Bargmann, 1998 Odorant receptor localization to olfactory cilia is mediated by ODR-4, a novel membrane-associated protein. Cell 93: 455–466.

Etchberger, J. F., A. Lorch, M. C. Sleumer, R. Zapf, S. J. Jones *et al.*, 2007 The molecular signature and cis-regulatory architecture of a C. elegans gustatory neuron. Genes Dev. 21: 1653–1674.

Fukuto, H. S., D. M. Ferkey, A. J. Apicella, H. Lans, T. Sharmeen *et al.*, 2004 G protein-coupled receptor kinase function is essential for chemosensation in C. elegans. Neuron 42: 581–593.

Gray, J. M., D. S. Karow, H. Lu, A. J. Chang, J. S. Chang *et al.*, 2004 Oxygen sensation and social feeding mediated by a C. elegans guanylate cyclase homologue. Nature 430: 317–322.

Guo, D., Y. C. Tan, D. Wang, K. S. Madhusoodanan, Y. Zheng *et al.*, 2007 A Rac-cGMP signaling pathway. Cell 128: 341–355.

Guo, D., J. J. Zhang, and X. Y. Huang, 2009 Stimulation of guanylyl cyclase-D by bicarbonate. Biochemistry 48: 4417–4422.

Hallem, E. A., W. C. Spencer, R. D. McWhirter, G. Zeller, S. R. Henz *et al.*, 2011 Receptor-type guanylate cyclase is required for carbon dioxide sensation by *Caenorhabditis elegans*. Proc. Natl. Acad. Sci. USA 108: 254–259.

Hobert, O., 2002 PCR fusion-based approach to create reporter gene constructs for expression analysis in transgenic C. elegans. Biotechniques 32: 728–730.

Hukema, R. K., 2006 Gustatory behaviour in Caenorhabditis elegans, pp. 176 in MGC Department of Cell Biology and Genetics. Erasmus MC, Rotterdam, The Netherlands.

Inada, H., H. Ito, J. Satterlee, P. Sengupta, K. Matsumoto *et al.*, 2006 Identification of guanylyl cyclases that function in thermosensory neurons of *Caenorhabditis elegans*. Genetics 172: 2239–2252.

Jansen, G., K. L. Thijssen, P. Werner, M. van der Horst, E. Hazendonk *et al.*, 1999 The complete family of genes encoding G proteins of Caenorhabditis elegans. Nat. Genet. 21: 414–419.

Jansen, G., D. Weinkove, and R. H. Plasterk, 2002 The G-protein gamma subunit gpc-1 of the nematode C.elegans is involved in taste adaptation. EMBO J. 21: 986–994.

Kaupp, U. B., and R. Seifert, 2002 Cyclic nucleotide-gated ion channels. Physiol. Rev. 82: 769–824.

Koch, K. W., T. Duda, and R. K. Sharma, 2002 Photoreceptor specific guanylate cyclases in vertebrate phototransduction. Mol. Cell. Biochem. 230: 97–106.

Komatsu, H., I. Mori, J. S. Rhee, N. Akaike, and Y. Ohshima, 1996 Mutations in a cyclic nucleotide-gated channel lead to abnormal thermosensation and chemosensation in C. elegans. Neuron 17: 707–718.

Lanjuin, A., M. K. VanHoven, C. I. Bargmann, J. K. Thompson, and P. Sengupta, 2003 Otx/otd homeobox genes specify distinct sensory neuron identities in C. elegans. Dev. Cell 5: 621–633.

L'Etoile, N. D., and C. I. Bargmann, 2000 Olfaction and odor discrimination are mediated by the C. elegans guanylyl cyclase ODR-1. Neuron 25: 575–586.

Letunic, I., T. Doerks, and P. Bork, 2012 SMART 7: recent updates to the protein domain annotation resource. Nucleic Acids Res. 40: D302–D305.

Lewis, J. A., and J. A. Hodgkin, 1977 Specific neuroanatomical changes in chemosensory mutants of the nematode Caenorhabditis elegans. J. Comp. Neurol. 172: 489–510.

Liu, J., A. Ward, J. Gao, Y. Dong, N. Nishio *et al.*, 2010 C. elegans phototransduction requires a G protein-dependent cGMP pathway and a taste receptor homolog. Nat. Neurosci. 13: 715–722.

Mori, I., and Y. Ohshima, 1995 Neural regulation of thermotaxis in Caenorhabditis elegans. Nature 376: 344–348.

Morton, D. B., 2004 Invertebrates yield a plethora of atypical guanylyl cyclases. Mol. Neurobiol. 29: 97–116.

Ortiz, C. O., J. F. Etchberger, S. L. Posy, C. Frokjaer-Jensen, S. Lockery *et al.*, 2006 Searching for neuronal left/right asymmetry: genomewide analysis of nematode receptor-type guanylyl cyclases. Genetics 173: 131–149.

Ortiz, C. O., S. Faumont, J. Takayama, H. K. Ahmed, A. D. Goldsmith *et al.*, 2009 Lateralized gustatory behavior of C. elegans is controlled by specific receptor-type guanylyl cyclases. Curr. Biol. 19: 996–1004.

Pierce-Shimomura, J. T., S. Faumont, M. R. Gaston, B. J. Pearson, and S. R. Lockery, 2001 The homeobox gene lim-6 is required for distinct chemosensory representations in C. elegans. Nature 410: 694–698.

Potter, L. R., 2011 Guanylyl cyclase structure, function and regulation. Cell. Signal. 23: 1921–1926.

Pradel, E., Y. Zhang, N. Pujol, T. Matsuyama, C. I. Bargmann *et al.*, 2007 Detection and avoidance of a natural product from the

pathogenic bacterium Serratia marcescens by *Caenorhabditis elegans*. Proc. Natl. Acad. Sci. USA 104: 2295–2300.
Ramot, D., B. L. MacInnis, and M. B. Goodman, 2008 Bidirectional temperature-sensing by a single thermosensory neuron in C. elegans. Nat. Neurosci. 11: 908–915.
Ruiz, C., S. Gutknecht, E. Delay, and S. Kinnamon, 2006 Detection of NaCl and KCl in TRPV1 knockout mice. Chem. Senses 31: 813–820.
Ryu, W. S., and A. D. Samuel, 2002 Thermotaxis in Caenorhabditis elegans analyzed by measuring responses to defined Thermal stimuli. J. Neurosci. 22: 5727–5733.
Sarin, S., M. O'Meara M, E. B. Flowers, C. Antonio, R. J. Poole *et al*., 2007 Genetic screens for *Caenorhabditis elegans* mutants defective in left/right asymmetric neuronal fate specification. Genetics 176: 2109–2130.
Scott, K., 2005 Taste recognition: food for thought. Neuron 48: 455–464.
Sengupta, P., 2007 Generation and modulation of chemosensory behaviors in C. elegans. Pflugers Arch. 454: 721–734.
Suzuki, H., T. R. Thiele, S. Faumont, M. Ezcurra, S. R. Lockery *et al.*, 2008 Functional asymmetry in Caenorhabditis elegans taste neurons and its computational role in chemotaxis. Nature 454: 114–117.
Uchida, O., H. Nakano, M. Koga, and Y. Ohshima, 2003 The C. elegans che-1 gene encodes a zinc finger transcription factor required for specification of the ASE chemosensory neurons. Development 130: 1215–1224.
Ward, S., 1973 Chemotaxis by the nematode *Caenorhabditis elegans*: identification of attractants and analysis of the response by use of mutants. Proc. Natl. Acad. Sci. USA 70: 817–821.
Wasserman, S. M., M. Beverly, H. W. Bell, and P. Sengupta, 2011 Regulation of response properties and operating range of the AFD thermosensory neurons by cGMP signaling. Curr. Biol. 21: 353–362.
Wedel, B., and D. Garbers, 2001 The guanylyl cyclase family at Y2K. Annu. Rev. Physiol. 63: 215–233.

Communicating editor: P. Sengupta

GENETICS

Supporting Information
http://www.genetics.org/lookup/suppl/doi:10.1534/genetics.113.152660/-/DC1

Defining Specificity Determinants of cGMP Mediated Gustatory Sensory Transduction in *Caenorhabditis elegans*

Heidi K. Smith, Linjiao Luo, Damien O'Halloran, Dagang Guo, Xin-Yun Huang, Aravinthan D. T. Samuel, and Oliver Hobert

DOI: 10.1534/genetics.113.152660

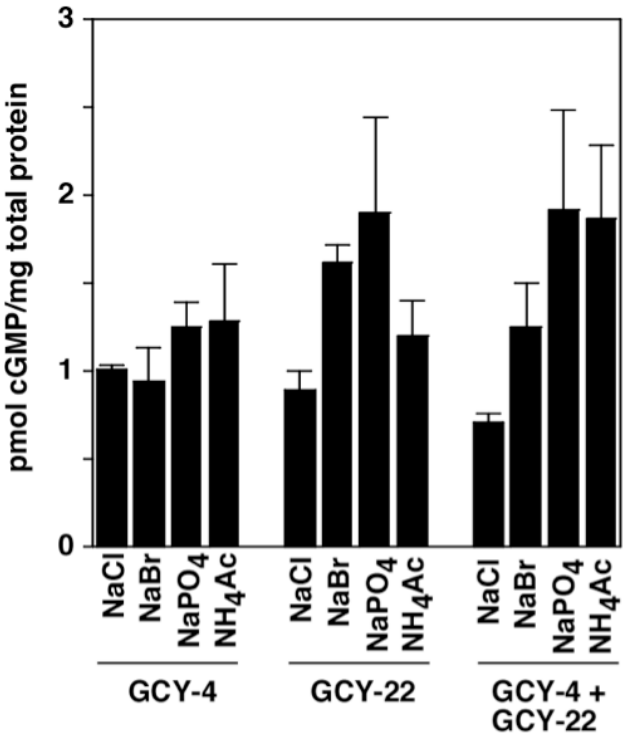

Figure S1 GCY-4 and GCY-22 do not show chloride, bromide, or sodium activation upon ectopic expression in CHO cells. Membrane preparations from CHO cells were treated with 100 mM NaCl, NaBr, $NaPO_4$, or NH_4Ac. cGMP levels were measured as pmol cGMP per mg of total membrane proteins. Comparing with the control (NH_4Ac), treatments with NaCl, NaBr or $NaPO_4$ did not produce a statistically significant stimulation of GC activity under the current experimental conditions. We also tested 100 mM NaI and observed no stimulation of GC activity. Protein expression was confirmed by Western Blotting, but we cannot be certain that proteins were transported to the cell surface.

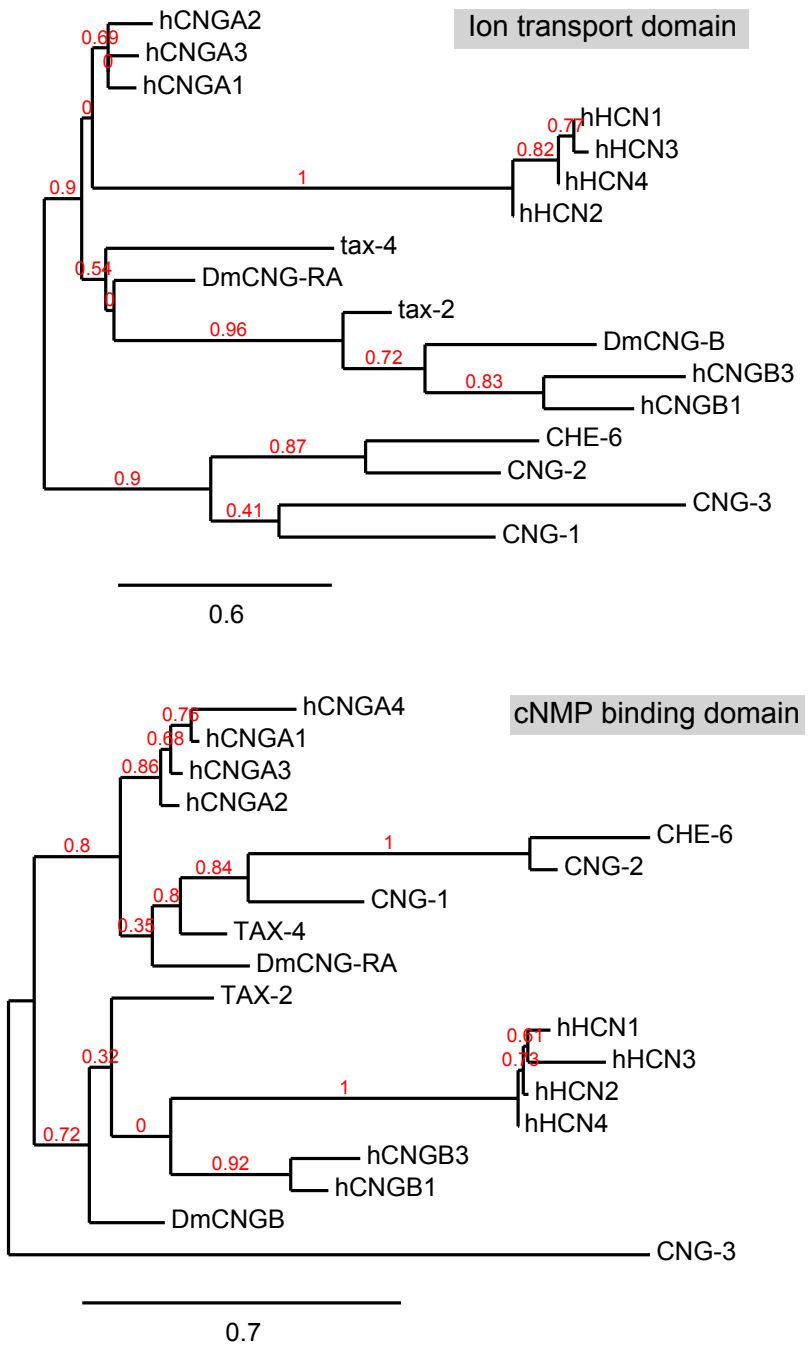

Figure S2 Phylogeny of CNG channels. (A) Phylogram of cNMP domain. (B) Phylogram of PF00520 Ion transport domain. The domains were defined by SMART database search and the phylogenetic tree was built with default parameters at the www.phylogeny.fr suite (Dereeper *et al.* 2008).

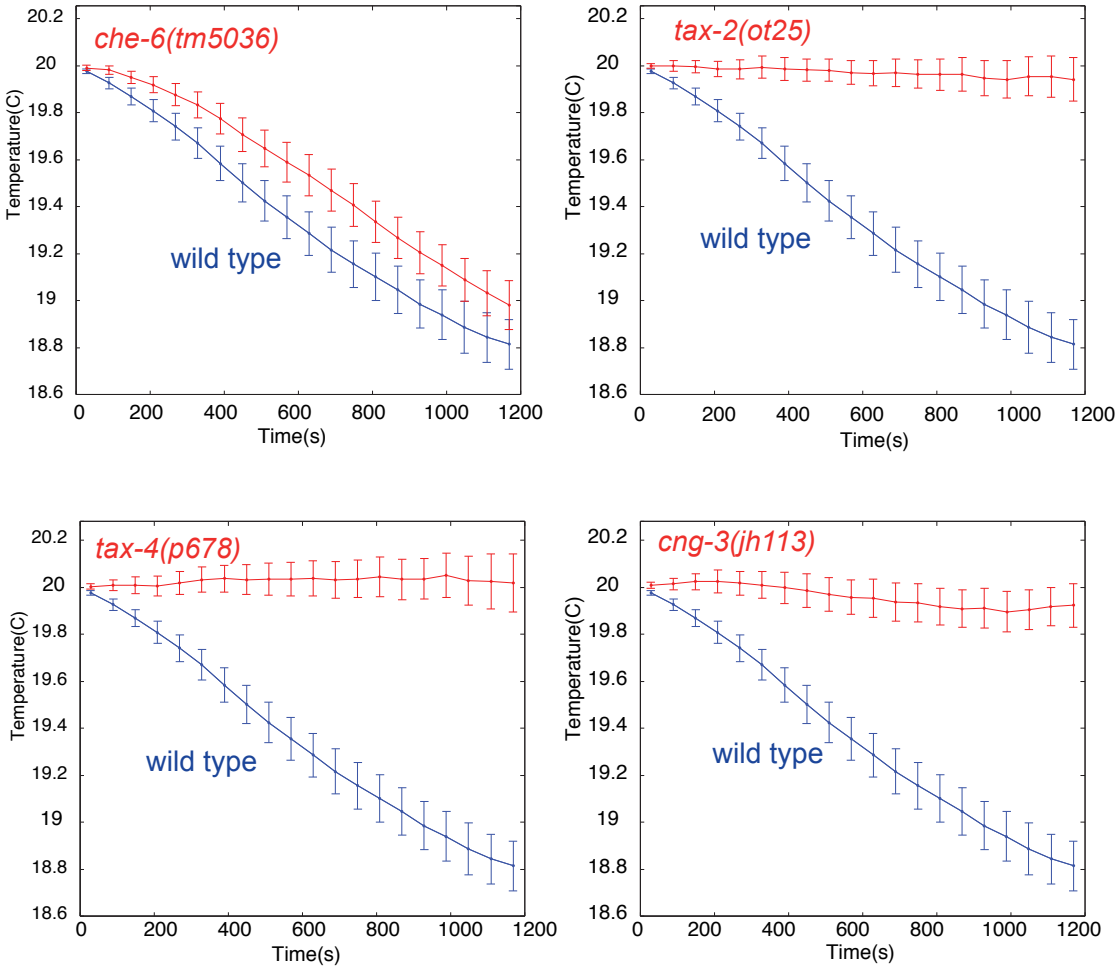

Figure S3 Alternative representation of thermotaxis data. Average horizontal positions for animals navigating the linear 0.2^{0}C/cm thermal gradients as described in Figure 9. Worms grown at 15˚C were started at 20˚C. Solid lines and error bars indicate the mean ±1 SEM of horizontal displacement from the start point over time measured over the trajectories of individual worms.

File S1

List of transgenic lines

Chimeric GCY receptor experiments:

OH11250 *gcy-1(tm2669)II; otEx5076* [FL *gcy-1; elt-2::gfp*]

OH11251 *gcy-1(tm2669)II; otEx5077* [pHKS019; *elt-2::gfp*], line #1

OH11252 *gcy-1(tm2669)II; otEx5078* [pHKS019; *elt-2::gfp*], line #2

OH11253 *gcy-1(tm2669)II; otEx5079* [pHKS019; *elt-2::gfp*], line #3

OH11254 *gcy-1(tm2669)II; otEx5080* [pHKS020; *elt-2::gfp*], line #1

OH11255 *gcy-1(tm2669)II; otEx5081* [pHKS020; *elt-2::gfp*], line #2

OH11256 *gcy-1(tm2669)II; otEx5082* [pHKS020; *elt-2::gfp*], line #3

OH11257 *gcy-1(tm2669)II; otEx5083* [pHKS018; *elt-2::gfp*], line #1

OH11258 *gcy-1(tm2669)II; otEx5084* [pHKS018; *elt-2::gfp*], line #2

OH11259 *gcy-1(tm2669)II; otEx5085* [pHKS018; *elt-2::gfp*], line #3

OH11260 *gcy-1(tm2669)II; otEx5086* [pHKS017; *elt-2::gfp*], line #1

OH11261 *gcy-1(tm2669)II; otEx5087* [pHKS017; *elt-2::gfp*], line #2

OH11262 *gcy-1(tm2669)II; otEx5088* [pHKS017*; elt-2::gfp*], line #3

OH11286 *gcy-4(tm1653)II; otEx5101* [FL *gcy-4; elt-2::gfp*]

OH11287 *gcy-4(tm1653)II; otEx5102* [pHKS015; *elt-2::gfp*], line #1

OH11288 *gcy-4(tm1653)II; otEx5103* [pHKS015; *elt-2::gfp*], line #2

OH11289 *gcy-4(tm1653)II; otEx5104* [pHKS015; *elt-2::gfp*], line #3

OH11290 *gcy-4(tm1653)II; otEx5105* [pHKS016; *elt-2::gfp*], line #1

OH11291 *gcy-4(tm1653)II; otEx5106* [pHKS016; *elt-2::gfp*], line #2

OH11292 *gcy-4(tm1653)II; otEx5107* [pHKS016; *elt-2::gfp*], line #3

OH11293 *gcy-4(tm1653)II; otEx5086* [pHKS017; *elt-2::gfp*], line #1

OH11294 *gcy-4(tm1653)II; otEx5087* [pHKS017; *elt-2::gfp*], line #2

OH11295 *gcy-4(tm1653)II; otEx5088* [pHKS017; *elt-2::gfp*], line #3

OH11296 *gcy-4(tm1653)II; otEx5083* [pHKS018; *elt-2::gfp*], line #1

OH11297 *gcy-4(tm1653)II; otEx5084* [pHKS018; *elt-2::gfp*], line #2

OH11298 *gcy-4(tm1653)II; otEx5085* [pHKS018; *elt-2::gfp*], line #3

OH11324 *gcy-22(tm2364)V; otEx5210* [FL *gcy-22; elt-2::gfp*]

OH11325 *gcy-22(tm2364)V; otEx5080* [pHKS020*; elt-2::gfp*], line #1

OH11326 *gcy-22(tm2364)V; otEx5081* [pHKS020; *elt-2::gfp*], line #2

OH11327 *gcy-22(tm2364)V; otEx5082* [pHKS020; *elt-2::gfp*], line #3

OH11328 *gcy-22(tm2364)V; otEx5077* [pHKS019; *elt-2::gfp*], line #1

OH11329 *gcy-22(tm2364)V; otEx5078* [pHKS019; *elt-2::gfp*], line #2

OH11330 *gcy-22(tm2364)V; otEx5079* [pHKS019; *elt-2::gfp*], line #3

OH11331 *gcy-22(tm2364)V; otEx5105* [pHKS016; *elt-2::gfp*], line #1

OH11332 *gcy-22(tm2364)V*; *otEx5106* [pHKS016; *elt-2::gfp*], line #2

OH11333 *gcy-22(tm2364)V; otEx5107* [pHKS016; *elt-2::gfp*], line #3

OH11334 *gcy-22(tm2364)V; otEx5102* [pHKS015; *elt-2::gfp*], line #1

OH11335 *gcy-22(tm2364)V; otEx5103* [pHKS015; *elt-2::gfp*], line #2

OH11336 *gcy-22(tm2364)V; otEx5104* [pHKS015; *elt-2::gfp*], line #3

Pansensory heterologous expression:

OH11231 *gcy-4(tm1653)II; otEx5067* [pHKS013; *elt-2::DsRed*], line #1

OH11232 *gcy-4(tm1653)II; otEx5068* [pHKS013; *elt-2::DsRed*], line #2

OH11233 *gcy-4(tm1653)II; otEx5069* [pHKS013; *elt-2::DsRed*], line #3

OH11230 *gcy-4(tm1653)II; otIs398* [pHKS013; *elt-2::DsRed*]

OH11234 *gcy-22(tm2364)V; otEx5070* [pHKS014; *elt-2::gfp*],line #1

OH11235 *gcy-22(tm2364)V; otEx5071* [pHKS014; *elt-2::gfp*], line #2

OH11236 *gcy-22(tm2364)V; otEx5072* [pHKS014; *elt-2::gfp*], line#3

OH11237 *che-1(ot66)I; otIs398* (integrated *otEx5068*) [pHKS013; *elt-2::DsRed*]

OH11239 *che-1(ot66)I; otEx5071* [pHKS014; *elt-2::gfp*]

OH11242 *che-1(ot66)I; otIs398 otEx5071*

ASI heterologous expression:

OH11783 *che-1(ot66)I; otEx5349 [pHKS031; myo-2::gfp],* line #1

OH11785 *che-1(ot66)I; otEx5351 [pHKS031; myo-2::gfp],* line #2

OH11786 *che-1(ot66)I; otEx5352 [pHKS031; myo-2::gfp],* line #3

OH11787 *che-1(ot66)I; otEx5353 [pHKS032; myo-2::gfp],* line #1

OH11788 *che-1(ot66)I; otEx5354 [pHKS032; myo-2::gfp],* line #2

OH11789 *che-1(ot66)I; otEx5355 [pHKS032; myo-2::gfp],* line #3

OH11793 *che-1(ot66)I; otEx5359 [pHKS031,pHKS032; myo-2::gfp],* line #1

OH11794 *che-1(ot66)I; otEx5360 [pHKS031,pHKS032; myo-2::gfp],* line #2

OH11795 *che-1(ot66)I; otEx5361 [pHKS031,pHKS032; myo-2::gfp],* line #3

***che-7* mutant analysis**

OH11226 *che-7(e1128)V; otEx5063* [*che-7*^{fosmid}; *elt-2::gfp*]

***che-6* mutant analysis**

OH11227 *che-6(e1126)IV; otEx5064* [FL *che-6; elt-2::gfp*], line #1

OH1128 *che-6(e1126)IV; otEx5065* [FL *che-6 ; elt-2::gfp*], line #2

OH1129 *che-6(e1126)IV; otEx5066* [FL *che-6; elt-2::gfp*], line #3

OH11380 *che-6(e1126)IV; otEx5154* [pHKS021; *elt-2::gfp*], line #1

OH11381 *che-6(e1126)IV; otEx5155* [pHKS021; *elt-2::gfp*], line #2

OH11382 *che-6(e1126)IV; otEx5156* [pHKS021; *elt-2::gfp*], line #3